

**CARBON AND ELECTRON FLOW VIA METHANOGENESIS,
SO₄²⁻, NO₃⁻, AND Fe³⁺ REDUCTION IN THE ANOXIC
HYPOLIMNIA OF UPPER MYSTIC LAKE**

by

Eliza J.R. Peterson

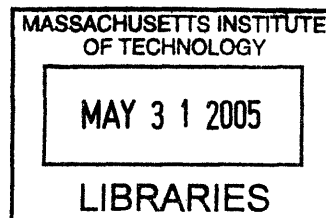
B.S. Microbiology
University of Michigan, 2002

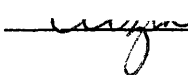
SUBMITTED TO THE DEPARTMENT OF CIVIL AND ENVIRONMENTAL
ENGINEERING IN PARTIAL FULFILLMENT OF THE REQUIREMENTS FOR THE
DEGREE OF

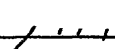
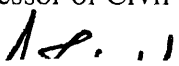
MASTER OF SCIENCE IN CIVIL AND ENVIRONMENTAL ENGINEERING
AT THE
MASSACHUSETTS INSTITUTE OF TECHNOLOGY


JUNE 2005

© 2005 Massachusetts Institute of Technology
All rights reserved



Signature of Author: 
Department of Civil and Environmental Engineering
May 12, 2005

Certified by: 
Harold Hemond
Professor of Civil and Environmental Engineering

Thesis Supervisor

Accepted by: 
Andrew J. Whittle
Professor of Civil and Environmental Engineering
Department Committee on Graduate Studies

ARCHIVES

CARBON AND ELECTRON FLOW VIA METHANOGENESIS, SO₄²⁻, NO₃⁻, AND Fe³⁺ REDUCTION IN THE ANOXIC HYPOLIMNIA OF UPPER MYSTIC LAKE

By

Eliza J.R. Peterson

Submitted to the Department of Civil and Environmental
Engineering on May 12, 2005 in Partial Fulfillment of the
Requirements for the Degree of Master of Science in Civil
and Environmental Engineering

ABSTRACT

The profiles of CH₄ and CO₂ obtained by the use of a novel sampler, along with the profiles for nitrate (NO₃⁻), sulfate (SO₄³⁻) and iron (Fe²⁺) were used to estimate the rates of the various anaerobic decomposition reactions during spring and fall stratification in Upper Mystic Lake. The equivalent electron and carbon flow of the reactions were also calculated to obtain a mass balance within the hypolimnia of UML. From the calculations, the approximate organic carbon decomposition rate, measured as CO₂ accumulation, was 7.54 mmol m⁻² d⁻¹. The amount of decomposition from the reactions involving nitrate, sulfate, iron and methane formation together accounted for 80% of the total organic carbon decomposition. Therefore, 20% of the CO₂ accumulation in UML could not be accounted for. Possible explanations for the excess CO₂ production could be the formation of reduced iron minerals and/or the loss of methane due to ebullition and oxidation. Such explanations suggest future studies of UML to better resolve the electron budget.

In order to study the redox balance in Upper Mystic Lake, a method was devised for precisely sampling dissolved gases in the water column. Like other stratified lakes, UML has a large amount of anaerobic metabolism of organic matter occurring in the sediments and a subsequent accumulation of methane (CH₄) and carbon dioxide (CO₂) in the hypolimnia. Previously, limnological sampling for dissolved gases involved filling glass bottles with water pumped from depth using a peristaltic pump; however, such methods introduce the potential for gas exchange with the atmosphere. Therefore, there was a need for a dissolved gas sampler that could be used to obtain samples at precise depth intervals while at the same time isolating the samples from outside influences.

Thesis Supervisor: Harold Hemond

Title: Professor of Civil and Environmental Engineering

ACKNOWLEDGEMENTS

My sincerest and deepest thanks go to my advisor, Professor Harry Hemond, with whom it was a pleasure and privilege to work. His combination of intellect, kindness, and humor is incredible. I am very appreciative of the opportunity afforded me to work with him and on Upper Mystic Lake.

I am also indebted to Larry Linden and the Martin Family for Linden and Martin Fellowships.

I have enjoyed my time and knowing many people at the Parsons Lab; several deserve special gratitude for their help and friendship: Katherine Lin, Janet Chuang, Matt Orosz, and Terry Donoghue. I would also like to acknowledge a UROP assistant, Elizabeth Walker for her help with sulfate analysis. In addition, Dr. John Durant, Michele Cutrofello, and Theresa McGovern of Tufts University deserve recognition for their collaboration with the Tufts Nutrient Project.

Above all, this thesis would not have been completed without a vast amount of love and support from my family, especially from my parents, Jane and Paul Peterson; my sister, brother-in-law and niece, Amy, Jeff and Ana Dunfee, and my sister, Carrie Peterson.

TABLE OF CONTENTS

Abstract.....	2
Acknowledgements.....	3
Table of Contents.....	4
List of Figures.....	6
List of Tables.....	7
 I. Introduction.....	 9
II. Study Site.....	12
III. Methods.....	14
Limnological Sampling.....	14
Nitrate, Sulfate and Ammonium.....	14
Iron (II).....	15
Methane and Carbon Dioxide.....	15
IV. Calculations.....	23
V. Results.....	26
T, O ₂ , pH and Conductivity Profiles.....	26
Inorganic Nitrogen Profiles.....	30
Fe ²⁺ Profiles.....	33
SO ₄ ²⁻ Profiles.....	35
CH ₄ and CO ₂ Profiles.....	38
Rates of Decomposition and Reduction of Electron Acceptors.....	41
Uncertainty in Rate Estimates.....	46
Electron Budget.....	47

Carbon Flow.....	49
VI. Discussion.....	51
Comparison to Other Lakes.....	51
Possible Explanations for the Electron Imbalance.....	54
VII. Conclusion.....	57
VIII. Appendix A.....	58
The Dissolved Gas Sampler.....	58
IX. Appendix B.....	67
Summary of Limnological Data.....	67
References.....	94

LIST OF FIGURES

Figure 1: Upper Mystic Lake bathymetry.....	13
Figure 2: Acidified vs. non-acidified CO ₂ samples.....	18
Figure 3: Chromatogram of lower column.....	19
Figure 4: Chromatogram of upper column.....	20
Figure 5: CH ₄ standard comparison.....	21
Figure 6: CO ₂ standard comparison.....	22
Figure 7: Temperature Profiles.....	27
Figure 8: Temperature Contour.....	28
Figure 9: Dissolved Oxygen Profiles.....	29
Figure 10: NH ₄ ⁺ Profiles.....	31
Figure 11: NO ₃ ⁻ Profiles.....	32
Figure 12: Fe ²⁺ Profiles.....	34
Figure 13: SO ₄ ²⁻ Profiles.....	36
Figure 14: CH ₄ Profiles.....	39
Figure 15: CO ₂ Profiles.....	40
Figure 16: Change in hypolimnetic mass of CO ₂ , CH ₄ during 110 day sampling period.....	42
Figure 17: Change in hypolimnetic mass of O ₂ , NO ₃ ⁻ , SO ₄ ²⁻ , Fe ²⁺ during 110 day sampling period.....	43
Figure A-1: The Dissolved Gas Sampler Diagram.....	63
Figure A-2: The Dissolved Gas Sampler.....	64
Figure A-3: Syringe “dock”.....	65
Figure A-4: 1-Sep-04 Replicate Samples.....	66

LIST OF TABLES

Table 1: Oxidation-reduction reactions involving the decomposition of organic matter.....	11
Table 2: UML bathymetry data used for mass balance calculations.....	25
Table 3: Late September 2004 storm data.....	37
Table 4: Rates of change of hypolimnetic species.....	44
Table 5: Comparison of CO ₂ accumulation in other lakes.....	45
Table 6: Reducing equivalents necessary to reduce the molar quantities of electron acceptors.....	48
Table 7: Carbon equivalents produced during the reduction of electron acceptors.....	50
Table 8: Comparison of overall electron budget from several lakes.....	52
Table 9: Comparison of electron acceptors as percent of CO ₂ accumulation for the Canadian experimental lakes.....	53
Table A-1: Cost and parts list for sampler.....	66
Table B-1: 13-May-04 Profile.....	68
Table B-2: 27-May-04 Profile.....	69
Table B-3: 10-Jun-04 Profile.....	70
Table B-4: 23-Jun-04 Profile.....	71
Table B-5: 7-Jul-04 Profile.....	72
Table B-6: 21-Jul-04 Profile.....	73
Table B-7: 4-Aug-04 Profile.....	74
Table B-8: 4-Aug-04 Profile continued.....	75
Table B-9: 18-Aug-04 Profile.....	76
Table B-10: 18-Aug-04 Profile continued.....	77
Table B-11: 1-Sep-04 Profile.....	78
Table B-12: 1-Sep-04 Profile continued.....	79

Table B-13: 15-Sep-04 Profile.....	80
Table B-14: 15-Sep-04 Profile continued.....	81
Table B-15: 1-Oct-04 Profile.....	82
Table B-16: 1-Oct-04 Profile continued.....	83
Table B-17: 15-Oct-04 Profile.....	84
Table B-18: 15-Oct-04 Profile continued.....	85
Table B-19: 27-Oct-04 Profile.....	86
Table B-20: 27-Oct-04 Profile continued.....	87
Table B-21: 10-Nov-04 Profile.....	88
Table B-22: 10-Nov-04 Profile continued.....	89
Table B-23: 22-Nov-04 Profile.....	90
Table B-24: 22-Nov-04 Profile continued.....	91
Table B-25: 15-Dec-04 Profile.....	92
Table B-26: 15-Dec-04 Profile continued.....	93

I. INTRODUCTION

The cycling of energy, carbon and nutrients in lake ecosystems is dependent on the decomposition of organic matter. In lake hypolimnia, decomposition is a dominant process and strongly influences the chemical constituents therein. The decomposition of organic matter involves microbial reactions that consume electron acceptors (e.g. O_2 , NO_3^- , SO_4^{3-} , Fe^{3+}) and produce CO_2 and CH_4 (Table 1; Kalff, 2002). During thermal stratification, the redox reactions involved in the decomposition of organic matter can be studied in essentially a “control volume” within the lower portion, or hypolimnion of a lake which is isolated from atmospheric exchange. Furthermore, when lakes are thermally stratified, the transport of metabolic end products from the hypolimnion to the upper portion (the epilimnion), and the downward diffusion of oxygen and other electron acceptors into the hypolimnion is small (Mattson and Likens, 1993; Houser J et al., 2003). Thus, hypolimnetic concentrations of oxygen and other electron acceptors typically decrease over the course of the stratified season while CO_2 , CH_4 , and the reduced end products accumulate.

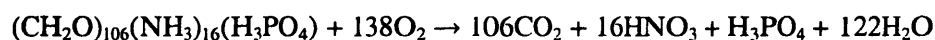
The anoxic hypolimnion of a stratified lake represents an environment where decomposition of organic matter only proceeds by anaerobic processes. In this environment, methanogenesis as well as nitrate, sulfate and iron reduction serve as the major reactions for the flow of electrons originally derived from reduced organic carbon. We describe here a method of estimating the extent of carbon and electron flow through

methanogenesis, nitrate, sulfate and iron reduction during anaerobic decomposition of organic matter in the hypolimnion of Upper Mystic Lake (UML; Medford, Massachusetts, USA) during the stratified period. This is done by constructing a mass balance model from changes in the vertical profiles of nitrate, sulfate, ferrous iron (Fe^{2+}) and methane during the entire sampling period.

Table 1. Oxidation-reduction reactions involving the decomposition of organic matter.

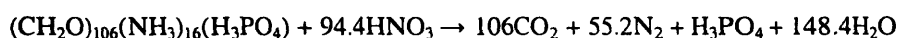
Table 1 includes the CO₂ equivalents and the maximum amount of free energy (ΔG_0) that can be derived from the reactions.

Reaction: Aerobic oxidation of organic matter



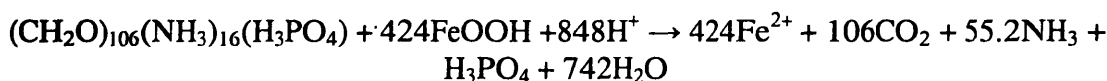
$$\begin{aligned}\text{O}_2:\text{CO}_2 &= -1 \\ \Delta G_0^* &= -3,190 \text{ kJmol}^{-1}\end{aligned}$$

Reaction: Denitrification



$$\begin{aligned}\text{NO}_3^-:\text{CO}_2 &= -1.25 \\ \Delta G_0^* &= -3,030 \text{ kJmol}^{-1}\end{aligned}$$

Reaction: Fe(III) Reduction



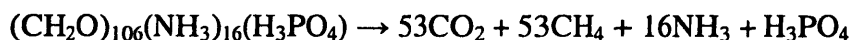
$$\begin{aligned}\text{Fe}^{2+}:\text{CO}_2 &= 0.25 \\ \Delta G_0^* &= -1,330 \text{ kJmol}^{-1}\end{aligned}$$

Reaction: Sulfate Reduction



$$\begin{aligned}\text{SO}_4^{2-}:\text{CO}_2 &= -2 \\ \Delta G_0^* &= -380 \text{ kJmol}^{-1}\end{aligned}$$

Reaction: Methanogenesis



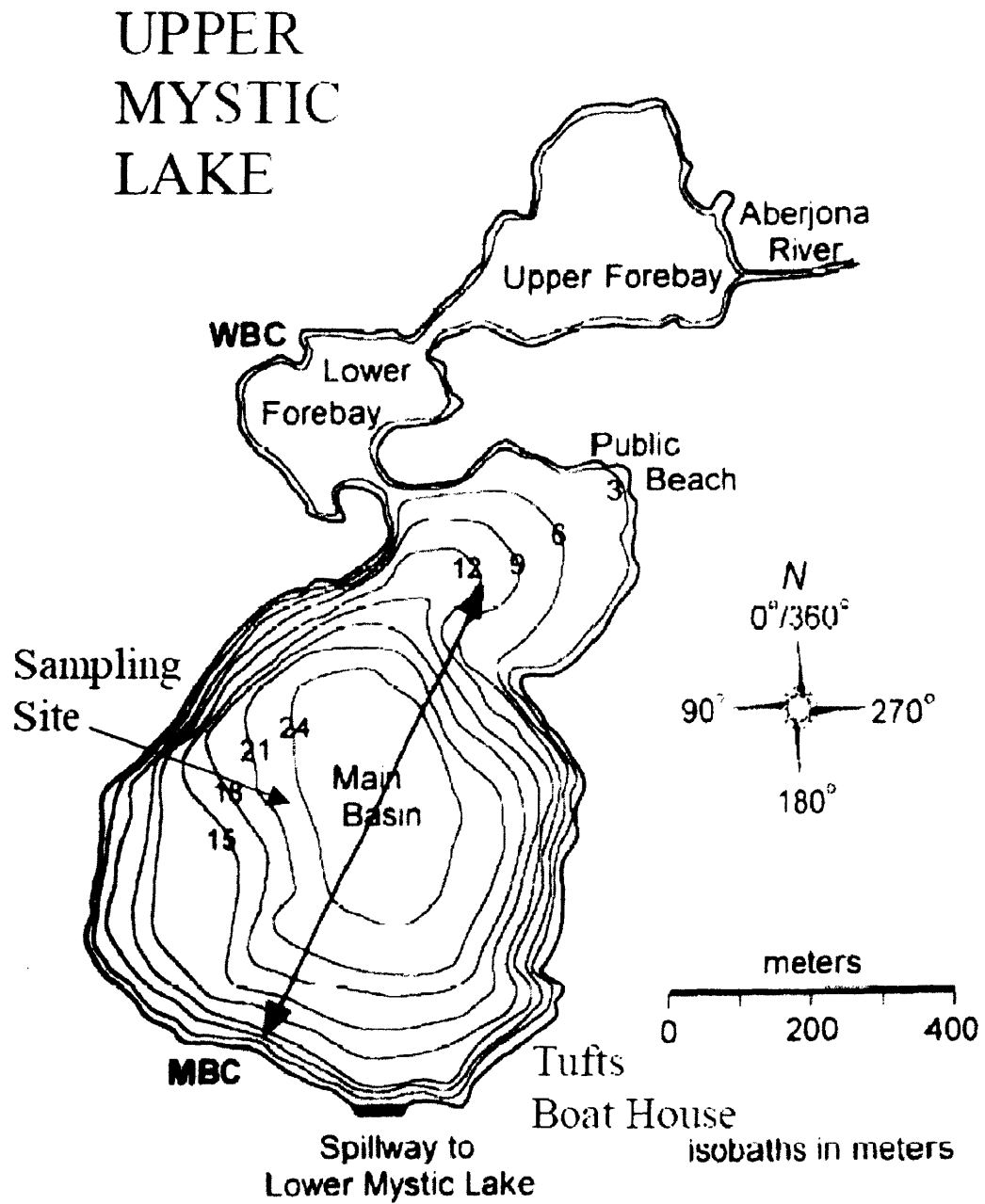
$$\begin{aligned}\text{CH}_4:\text{CO}_2 &= 1 \\ \Delta G_0^* &= -350 \text{ kJmol}^{-1}\end{aligned}$$

* ΔG_0 represents the change in standard free energy when 1 mole of reactant (represented here by organic matter with an average oxidation state corresponding to glucose) is converted to 1 mole of product (at 25°C, at 1 atm of pressure, and at a pH of 7).

II. STUDY SITE

This study was conducted at the Upper Mystic Lake in eastern Massachusetts, north of Boston (Figure 1). The Upper Mystic Lake is the outlet for the Aberjona Watershed and is a eutrophic, dimictic, kettlehole lake ($z_{\max} = 24$ m; $z_{\text{avg}} = 15$ m; $A_{\text{surface}} \sim 45$ ha; $V = 7 \times 10^6$ m³) (Senn 2002). The Aberjona River flows into the north end of the lake through two shallow forebays and at the south end there is a dam that controls the exit flow into the Lower Mystic Lake. The Aberjona Watershed received large quantities of metals, including arsenic (As) and chromium (Cr), during the early to mid-1900s as a result of leather and chemical manufacturing industries within its boundaries. Given that UML receives the entire flow of the Aberjona River, the lake has high levels of As in its sediments (Spliethoff and Hemond, H.F., 1996). Because of the high As concentrations, the remobilization and biogeochemistry of As has been studied extensively in UML (Aurilio et al., 1994; Spliethoff et al., 1995; Trowbridge 1995). Previous studies have observed that thermal stratification is established by late spring and by early summer, the hypolimnion is usually anoxic. During this study, sampling began mid May 2004, at which time the lake was already stratified and the hypolimnion was depleted of oxygen.

Figure 1. Bathymetry of UML



III. METHODS

Limnological Sampling

The water column of Upper Mystic Lake was monitored biweekly over the May to December interval of 2004 at a buoyed, deep water (~21 m) station. Dissolved oxygen (DO), temperature, pH and conductivity profiles (1 m intervals) were measured *in situ* using a submersible probe unit (Hydrolab MiniSonde); a pressure transducer in the probe unit determined depth.

Nitrate, Sulfate and Ammonium

For all sampling dates, water samples for nitrate, sulfate and ammonium were taken throughout the water column. Water samples were collected in 125 ml plastic Nalgene bottles by means of a peristaltic pump, with Tygon® tubing attached to the Hydrolab housing. Three volumes were allowed to overflow and the bottles were immediately capped, stored on ice and transported back to the lab where they were immediately frozen and preserved until analysis.

Samples for nitrate and sulfate were analyzed by ion chromatography (IC) with the following parameters: Dionex AS4A-SC column; Beckman autosampler 507; ASRS-1 suppressor; and 1.8 mM Na₂CO₃ + 1.7 mM NaHCO₃ eluent at ~1.3 ml min⁻¹. Nitrate and sulfate samples were analyzed on the IC with a conductivity scale of 10 µmho and 30

µmho, respectively. Ammonium samples were maintained frozen until colorimetric analysis by the phenolhypochlorite method (Solorzano 1969).

Iron (II)

From June 23, 2004 onward iron (Fe^{2+}) samples were taken from depths lower than 12 m. Samples were collected by the use of the tubing and pump described above, but water samples were transferred to 1.5 ml plastic centrifuge tubes containing 63 µl of concentrated hydrochloric acid. Samples were acidified to initiate the release of loosely bound, particle associated Fe^{2+} as well as to prevent Fe^{2+} oxidation. Additionally, sunlight can cause a significant reduction of Fe^{3+} to Fe^{2+} , therefore acidified samples were stored and transported in a dark box (Senn 2001). In the laboratory, 0.75 ml of the acidified sample was added to 0.75 ml of acetate buffer containing 1 g/L ferrozine (Stookey 1970). Absorbance ($\lambda = 562 \text{ nm}$) was measured in 1 cm disposable cuvettes.

Methane and Carbon Dioxide

From August to December, water samples to determine CH_4 and CO_2 concentrations were collected from the hypolimnion. Dissolved gas samples were obtained using a newly engineered sampling device that is described in Appendix A. Briefly, at each depth the sampler captured approximately 25 ml of water directly into a 50 ml glass syringes fitted with a 3-way Luer lok[®] valve. The filled syringes were stored under ice water for transport and analysis within 24 hours of sampling.

Methane and carbon dioxide concentrations were measured by gas chromatography using an F&M Scientific Corporation (Avondale, PA) instrument, equipped with a thermal conductivity detector (TCD). Methane and carbon dioxide

concentrations were determined using a headspace equilibration method, commonly used for measuring partial pressure of metabolic gases in water samples (Swinerton et al., 1962; Kampbell and Vandegrift, S., 1998). Headspace equilibration was performed by documenting the water volume in each syringe, injecting a recorded volume of helium (He) into each syringe, and placing the syringes for 30 minutes on a wrist-action shaker to allow the water and headspace gases to equilibrate. Samples taken on and after October 1, 2004 were acidified with ~25 μ l of 1N nitric acid to protonate bicarbonate ions, prior to He addition. A comparison of acidified versus non-acidified samples, collected on Oct 1, 2004 was used to correct previously analyzed CO₂ data (Figure 2). The partitioned headspace gases were then emptied into upper and lower sampling loops for injection onto columns having Molecular Sieve S and Hayspec C, respectively, as the packing material. Ultra-pure helium was used as the carrier gas, at a flow rate of 30 ml/min for the upper column and 18 ml/min for the lower column. CH₄ and CO₂ were detected by a thermal conductivity detector, and peak heights quantified by a Perkin Elmer Chart Recorder (Model PE056-1001). The lower column was used to separate CO₂ from other gases; CO₂ follows the composite mixture to be recorded as the second peak (Figure 3). The upper column then resolves the composite mixture; the separated gases emerge and are recorded in the order O₂, N₂ and CH₄ (Figure 4). Standards were made in reusable 35 L gas cylinders using certified CH₄ and CO₂ in He. The standards mixed in the lab were tested against Scotty Transportable® gases and replicate samples for CH₄ and CO₂ agreed within 2 percent and 7 percent, respectively (Figures 5 and 6). Peak heights for each gas were converted to partial pressures based on the standard

curves, Henry's law constant (Hemond and Fechner-Levy, E., 2000), water sample volume and headspace volume readings.

Figure 2. Acidified vs non-acidified CO₂ samples

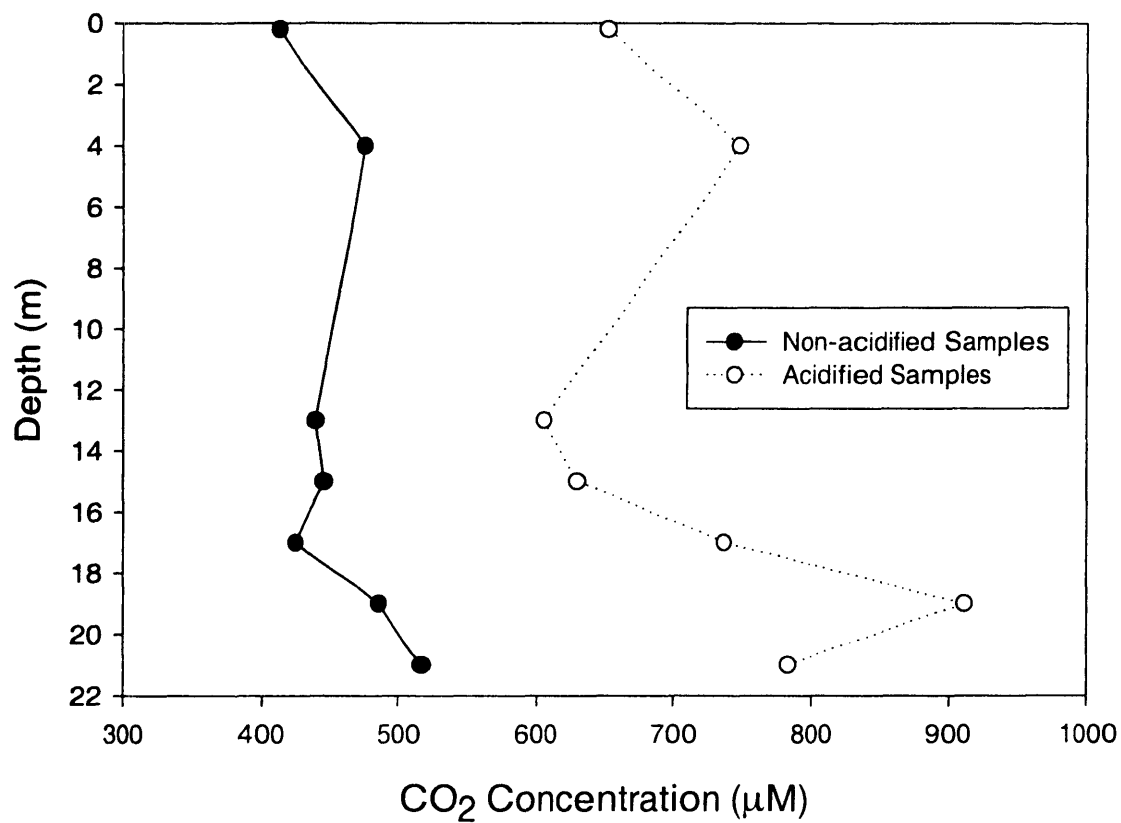


Figure 4. Chromatogram of Lower Column

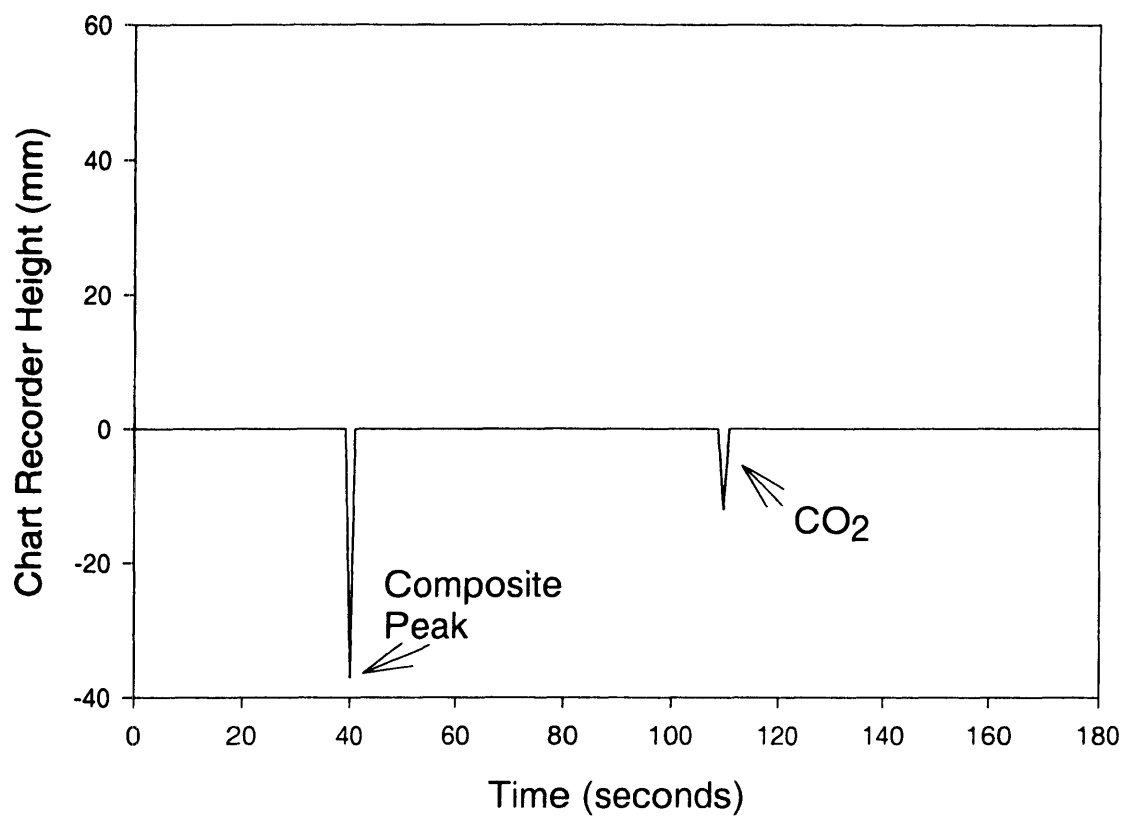


Figure 4. Chromatogram of Upper Column

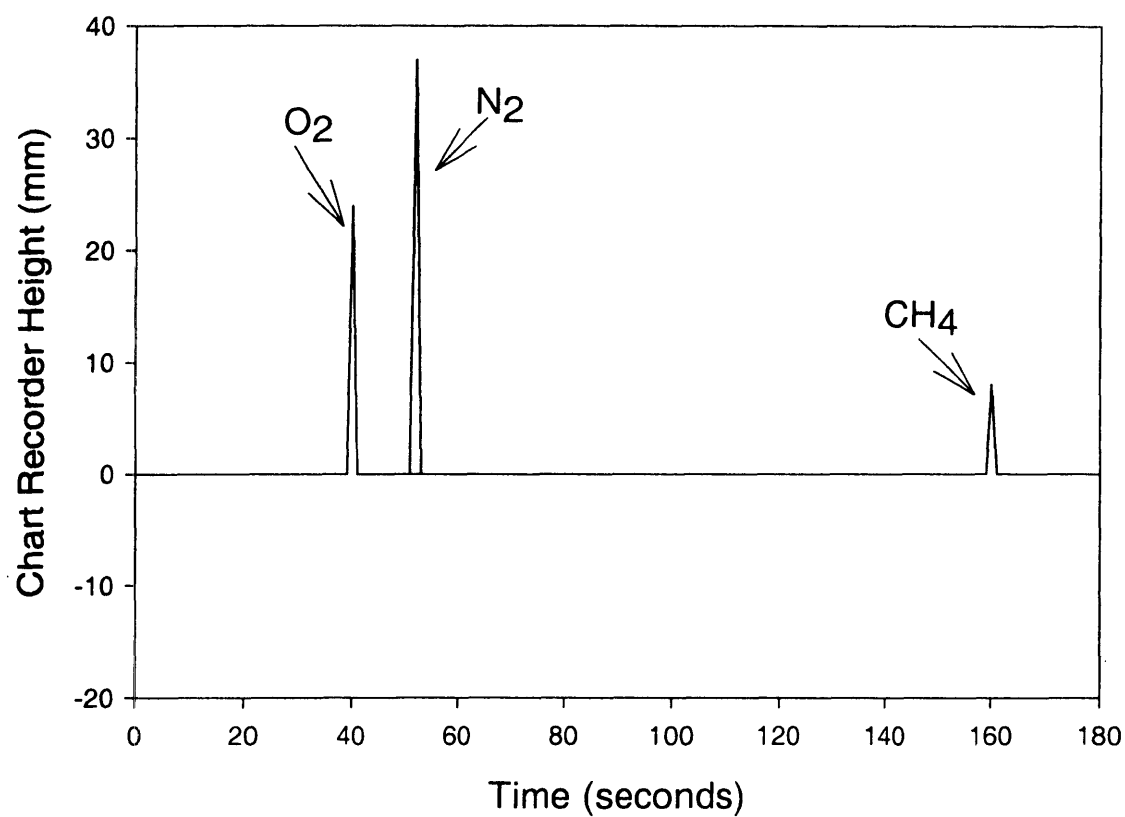


Figure 5. CH₄ Standard Comparison

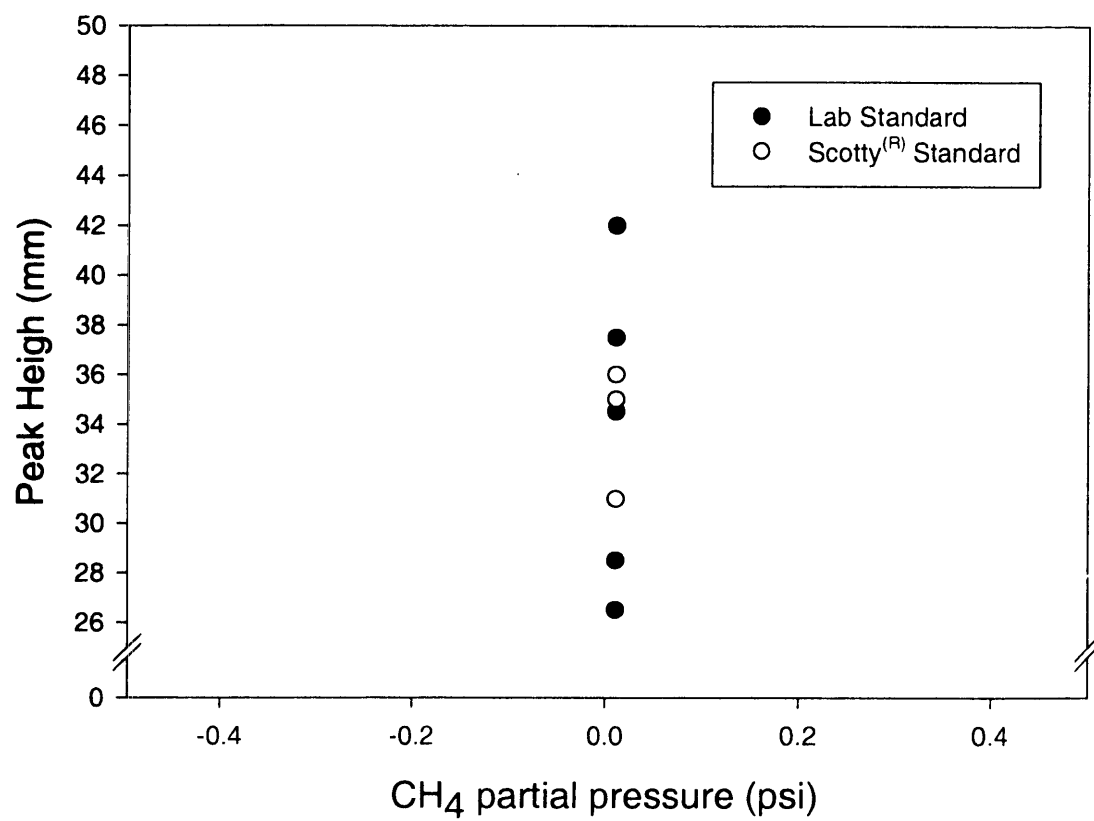
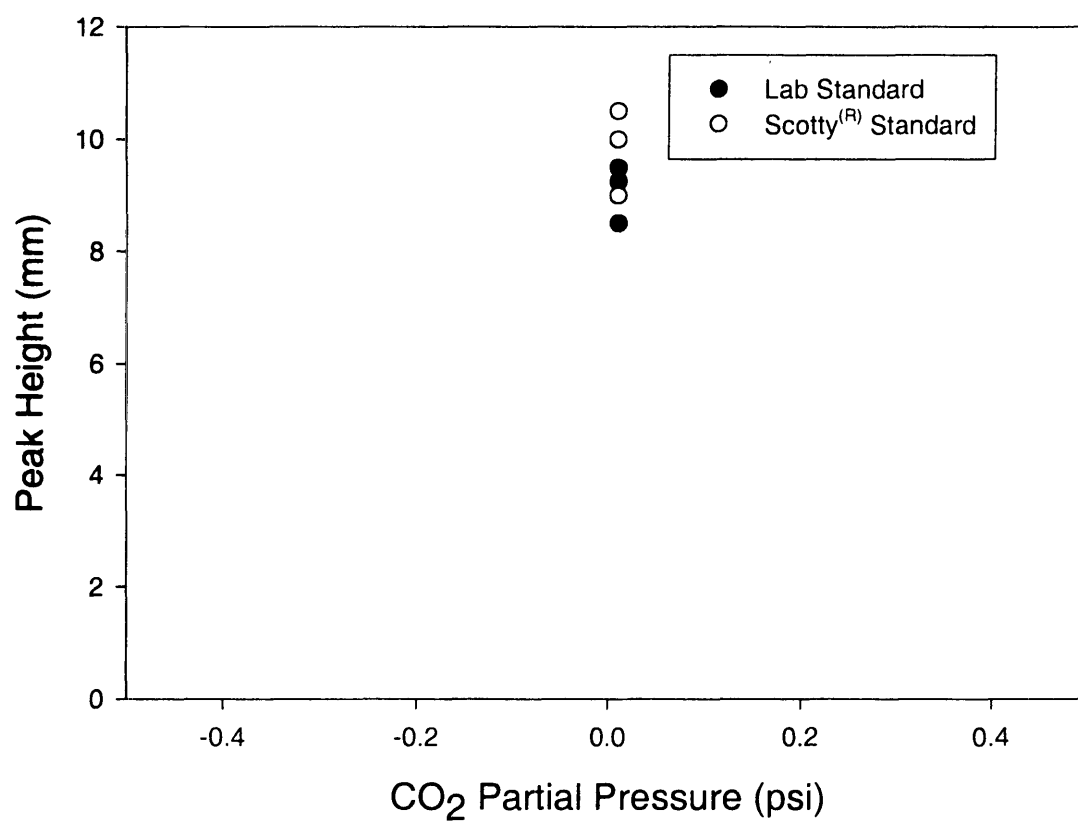


Figure 6. CO₂ Standard Comparison



IV. CALCULATIONS

To quantify the redox balance in UML's hypolimnion, the 15-20 m depth interval was considered the control volume. The 15-20 m control volume was chosen for the mass balance calculations because: i) the depth was clearly within the zone of CO₂ accumulation throughout the sampling period; ii) it was only necessary to consider diffusion across the 21 m surface (the other "boundaries" are the sediment-water interface); and iii) the most complete measurements were available for this region.

The masses of CO₂, CH₄, NO₃⁻, SO₄³⁻ and Fe²⁺ in the hypolimnion of UML were calculated as follows. The concentrations of each substance were linearly interpolated between the sampled depths at 1 m intervals. The concentration of a substance in each 1 m thick stratum was determined as the average of the concentration at the top and bottom of that stratum. The area at depth was determined from multiple bathymetric maps to the same 1 m intervals as the limnological data. UML bathymetry data used for the mass balance calculations are presented in Table 2. The volume of each 1 m thick stratum was determined assuming that each stratum could be represented as an irregular cone (Wetzel and Likens, 2000). Finally, the mass of each substance in that stratum was determined as the product of the volume of water in the stratum and the concentration of each substance.

The change in hypolimnetic mass ($\Delta Mass$) over the 110 day sampling period from August 4, 2004 to November 22, 2004 was calculated as follows:

$$\Delta Mass = Mass_2 - Mass_1 + D \quad (1)$$

Where $Mass_1$ is the mass contained in the hypolimnion (mmol m^{-2}) at the early sampling date, August 4, 2004 and $Mass_2$ is the mass contained in the hypolimnion at the late sampling date, November 22, 2004. D is the diffusive flux from the hypolimnion to the epilimnion. It was calculated using Fick's Law:

$$D = K \frac{\partial C}{\partial z} \quad (2)$$

where K is the coefficient of vertical eddy diffusion and $\frac{\partial C}{\partial z}$ (mmol m^{-4}) is the concentration gradient of the substance of interest at the control volume surface. Based on temperature gradient estimates for UML determined by Senn (2001), a $K = 0.02 \pm 0.01 \text{ cm}^2 \text{ s}^{-1}$ was used.

Table 2. UML bathymetry data used for mass balance calculations

Depth	Area*	Area†
M	10^5 m^2	10^5 m^2
0	5.83	5.00
3	4.19	3.57
6	3.67	3.09
9	3.19	2.70
12	2.7	2.30
15	2.06	1.74
18	1.62	1.39
21	1.2	1.04
24	0.7	0.52

Depth Interval	Volume
m	10^6 m^3
15-16	1.85
16-17	1.75
17-18	1.65
18-19	1.5
19-20	1.35

* from Spliethoff, 1995 (Areas determined by planimeter)

† from Xanat Flores, personal communication, 2004 (Areas determined by weighing contours)

V. RESULTS

T, O₂, pH and Conductivity Profiles

Temperature, dissolved oxygen, pH (Appendix B) and conductivity (Appendix B) measurements from 2004 were found to be consistent with previous UML studies (Aurilio et al., 1994; Spliethoff et al., 1995; Senn 2001). A well-established thermocline was evident on the first sampling date on May 13, 2005, at which time some oxygen depletion was also evident (Figure 7 and 8). Oxygen consumption continued through June, and oxygen levels were below detection in the deepest 12 meters by late July (Figure 9). Summer dissolved oxygen profiles had a local dissolved oxygen minimum at the thermocline, a feature also observed in previous years (Aurilio et al., 1994). A depth of 8-10 m below the surface represented the base of the thermocline throughout the summer and early-fall, with a gradual thermocline deepening over the course of the fall. The water column remained stratified, with the bottom ~8 meters unmixed, through the final sampling date of December 15, 2004. The pH measured above 8 in the epilimnion during the height of the summer, while hypolimnetic values ranged from 6.1 to 7.2. The average conductivity below 15 m was stable at 1.64 ± 0.2 mS/s, while the epilimnion had an average value of 0.58 ± 0.09 mS/s from the surface to ~11 m. There was a steep conductivity gradient at ~12 m that remained stable until late November, when the chemocline began to deepen.

Figure 7. Temperature Profiles

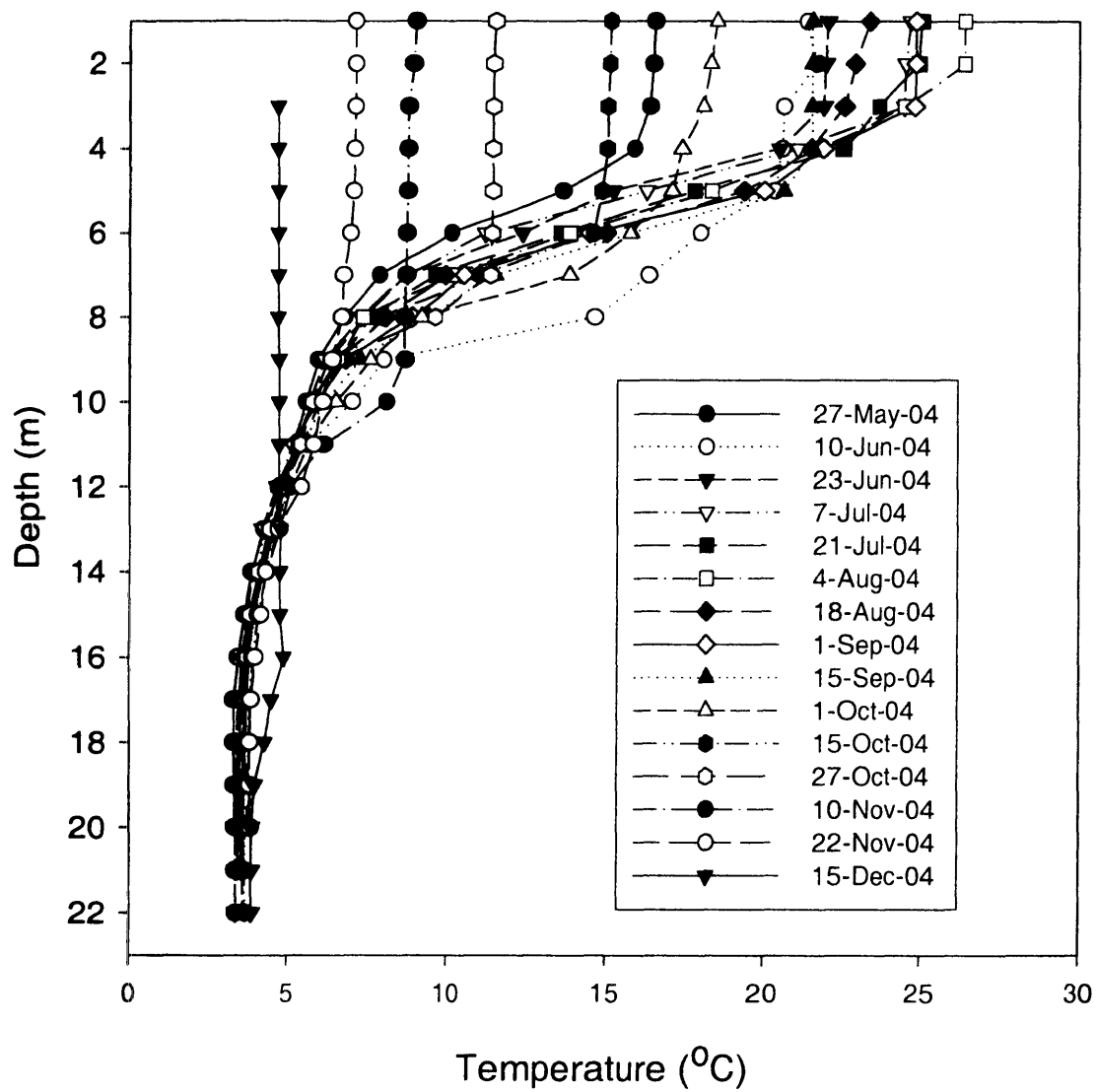


Figure 8. Temperature Contour

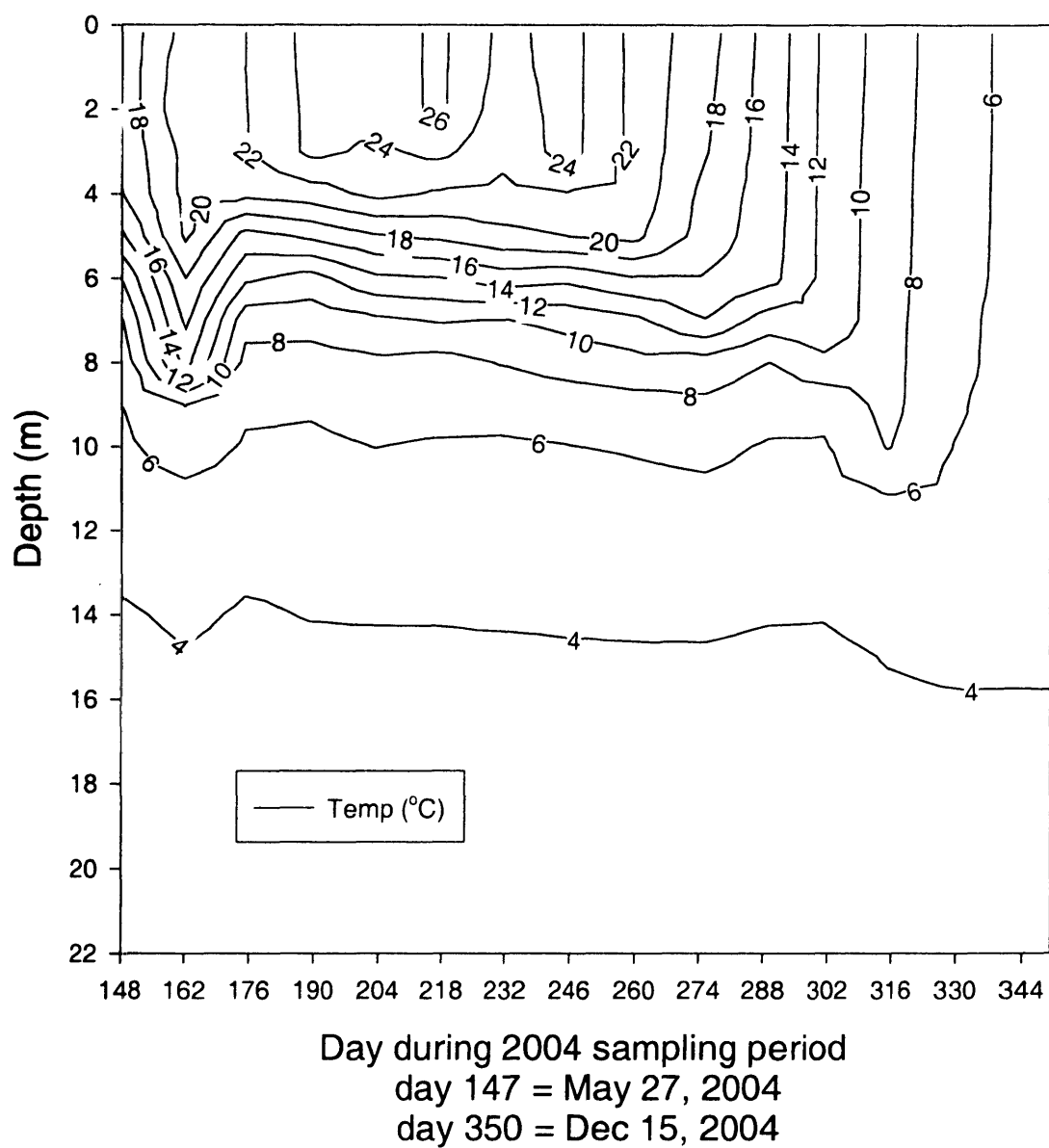
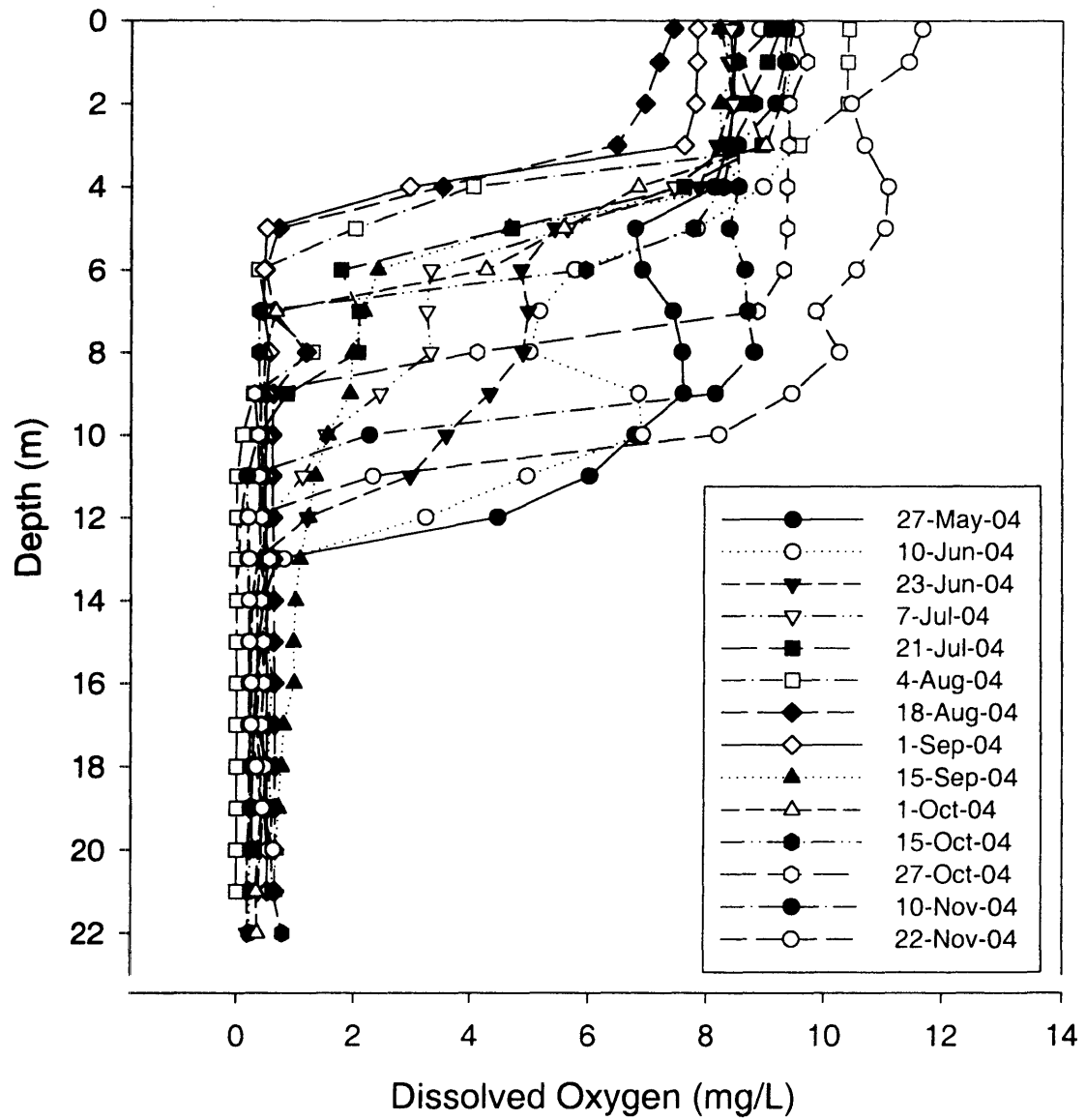
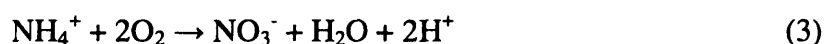


Figure 8. Dissolved Oxygen Profiles



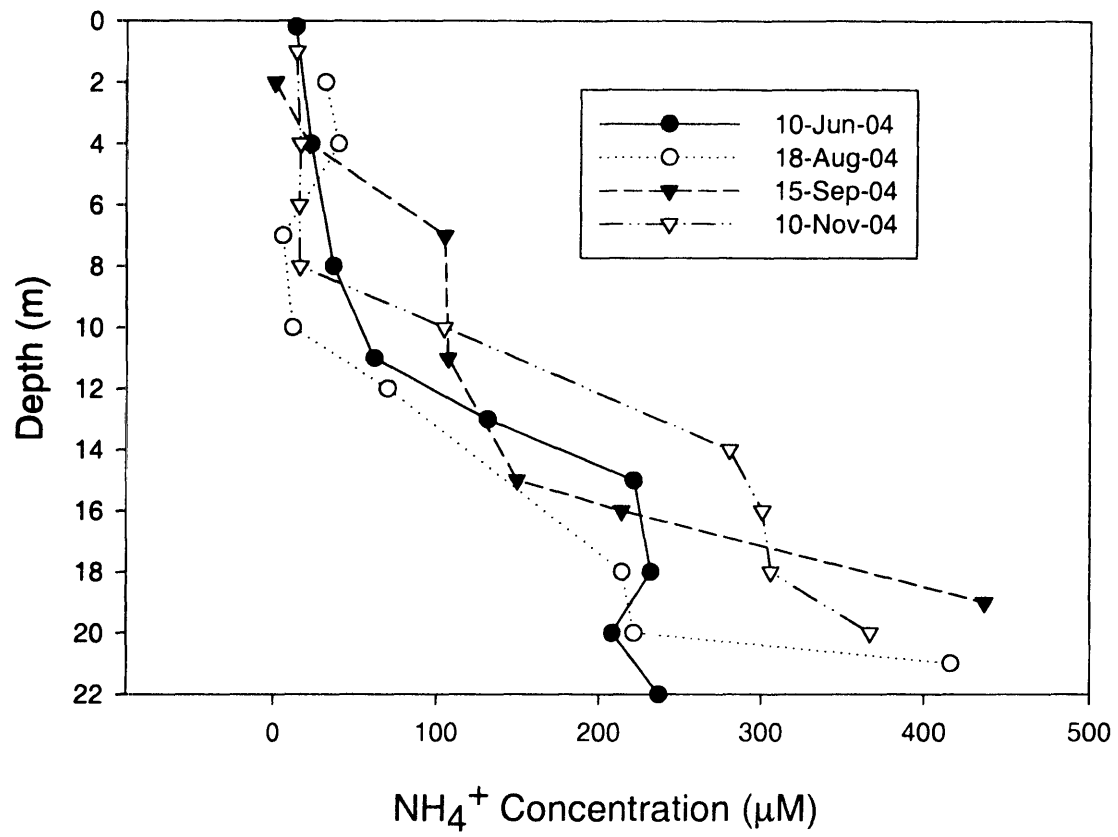
Inorganic Nitrogen Profiles

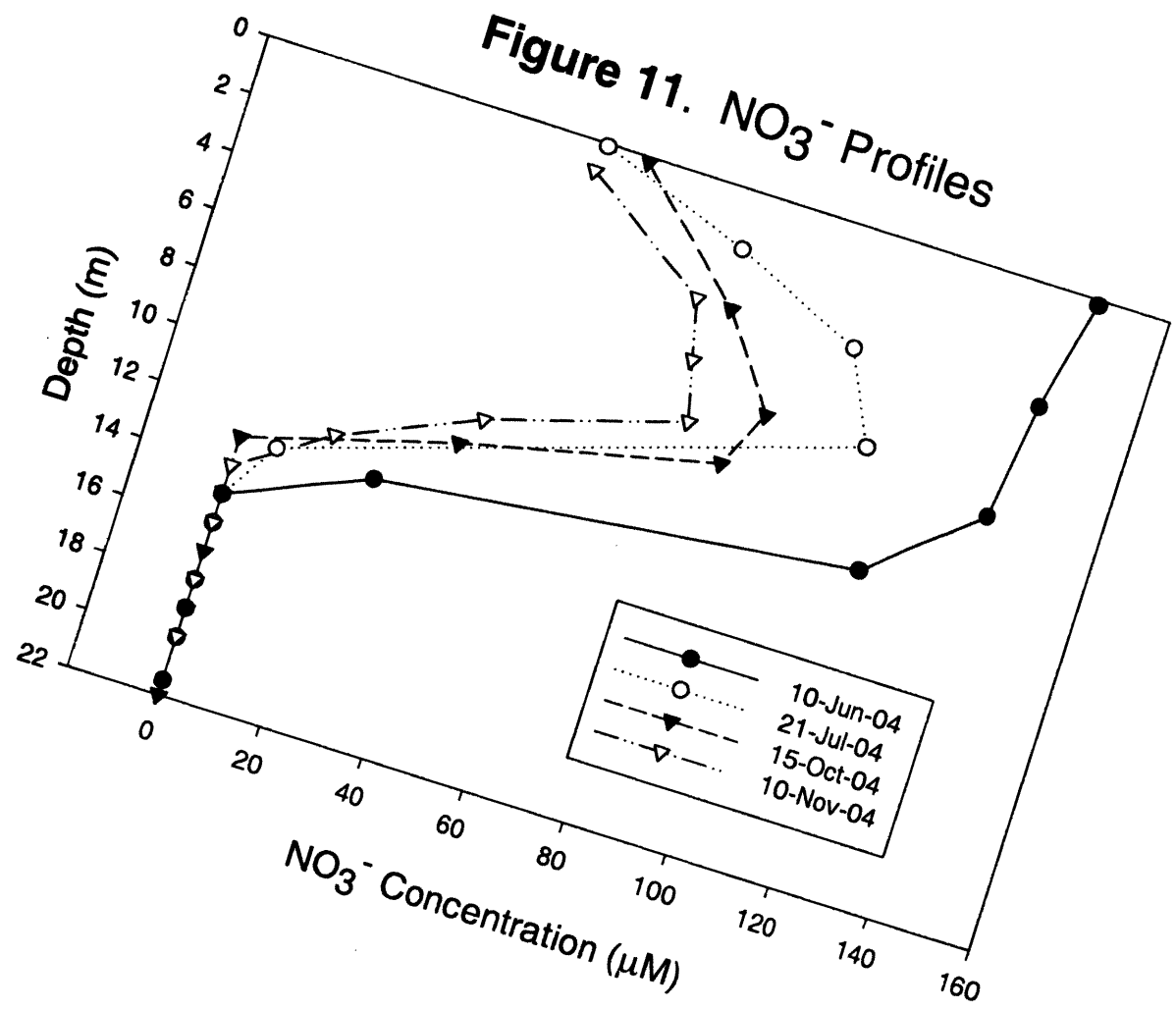
Nitrogen inputs (stormwater runoff, combined sewer overflows, and former industrial activities) occur along the Aberjona Watershed, resulting in elevated levels of ammonium (NH_4^+) and nitrate (NO_3^-) in UML (Senn 2001). From the beginning of sampling, a mid-depth (7-11 m) peak in nitrate concentrations was apparent, with NO_3^- levels frequently exceeding 100 μM . Deeper in the water column, nitrate disappeared and nitrate depletion in the hypolimnion was found from the onset of sampling. At the same time, NH_4^+ was found in high concentrations in the hypolimnion, as high as 600 μM at the sediment surface. Figures 10 and 11 display NH_4^+ and NO_3^- profiles from selected sampling dates, Appendix B presents complete Nitrogen data. The elevated levels of NH_4^+ in the hypolimnetic waters is most likely a result of NH_4^+ diffusion from the sediments where the breakdown and mineralization of organic matter (ammonification) is taking place (Kalff 2002). The NH_4^+ diffuses from the sediments, up through the water column, until it reaches the interface between oxic and anoxic waters (oxycline), where it is oxidized to NO_3^- (nitrification). The nitrification reaction,



consumes ammonium and oxygen, while producing nitrate. The nitrification process is most likely responsible for the mid-depth peak of NO_3^- and the DO minimum at the thermocline observed in UML. While equation (2) is a redox reaction and involves the transfer of electrons, the reaction occurs outside our control volume and therefore does not influence our mass balance. Furthermore, the absence of NO_3^- in the hypolimnion eliminates NO_3^- as a possible electron acceptor during the decomposition of organic matter.

Figure 10. NH_4^+ Profiles



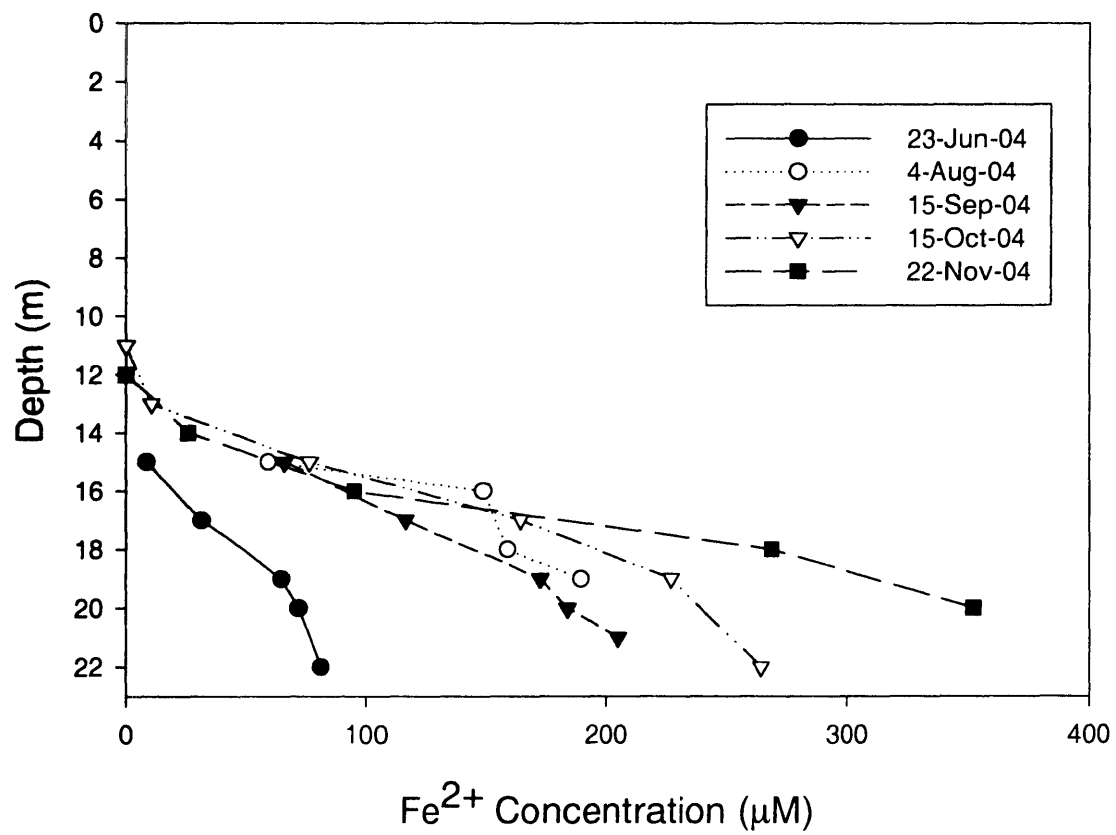


Fe²⁺ Profiles

The presence of Fe²⁺, measured as acid soluble Iron(II), was found below a depth of 13 m and concentrations increased linearly towards the sediments (Figure 12). Overall Fe²⁺ concentrations increased throughout the sampling period, reaching a maximum of ~350 µM in late November. The accumulation of Fe²⁺ in the hypolimnion comes from the oxidation of organic matter with the associated reduction of insoluble Fe³⁺ in the sediments. Insoluble Fe³⁺ oxides and oxyhydroxides settle onto the sediments and become subject to reduction, producing Fe²⁺ once the DO, manganese (Mn⁴⁺), and nitrate have been utilized as electron acceptors during the decomposition of organic matter. Such conditions prevailed in UML since DO and nitrate were never present in the hypolimnia during the sampling period; therefore, the production and accumulation of Fe²⁺ is reasonable.

It should be noted that manganese was not measured during this study, but was found to be negligible in UML by Senn 2001. In Senn's study of UML, acid-soluble manganese never exceeded concentrations of 20 µM, even at the deepest depths, and at such low levels Mn can be considered negligible in terms of the electron budget. Moreover, as an electron acceptor, Mn⁴⁺ provides more free energy and is preferentially reduced before NO₃⁻ in the ecological redox sequence; seeing that NO₃⁻ was depleted in UML, it is most likely that Mn⁴⁺ would have already been consumed and therefore not present in significant amounts.

Figure 12. Fe^{2+} Profiles



SO₄²⁻ Profiles

Sulfate profiles (Figure 13) resemble nitrate profiles in that concentrations decrease through the hypolimnion as SO_4^{2-} is used as an electron acceptor in the anaerobic decomposition of organic matter (Steenbergen et al., 1984). However, unlike NO_3^- , the complete depletion of sulfate in the hypolimnia did not happen during the sampling season. Hypolimnetic sulfate concentrations decreased linearly throughout the summer until Oct 1, 2004, when concentrations jumped back up to levels similar to the beginning of the summer and then decreased again. The cause of the sharp increase in sulfate concentrations is unknown. It is likely that reduced sulfides present in the samples could have oxidized during storage and added to the measured sulfate concentrations. It is also possible that a storm event that occurred just prior to the Oct 1, 2004 sampling date brought in large amounts of cold, SO_4^{2-} rich (average $\sim 125 \mu\text{M}$) water that underflowed into the hypolimnion (see Table 3 for storm data). Assuming this was the case, the storm event also brought in NO_3^- to the hypolimnion at an average concentration of $62 \mu\text{M}$; such low concentrations did not affect the mass balance. Alternatively, the NO_3^- brought in by the storm was most likely immediately reduced and therefore not observed in the nitrate profiles.

Figure 13. SO_4^{2-} Profiles

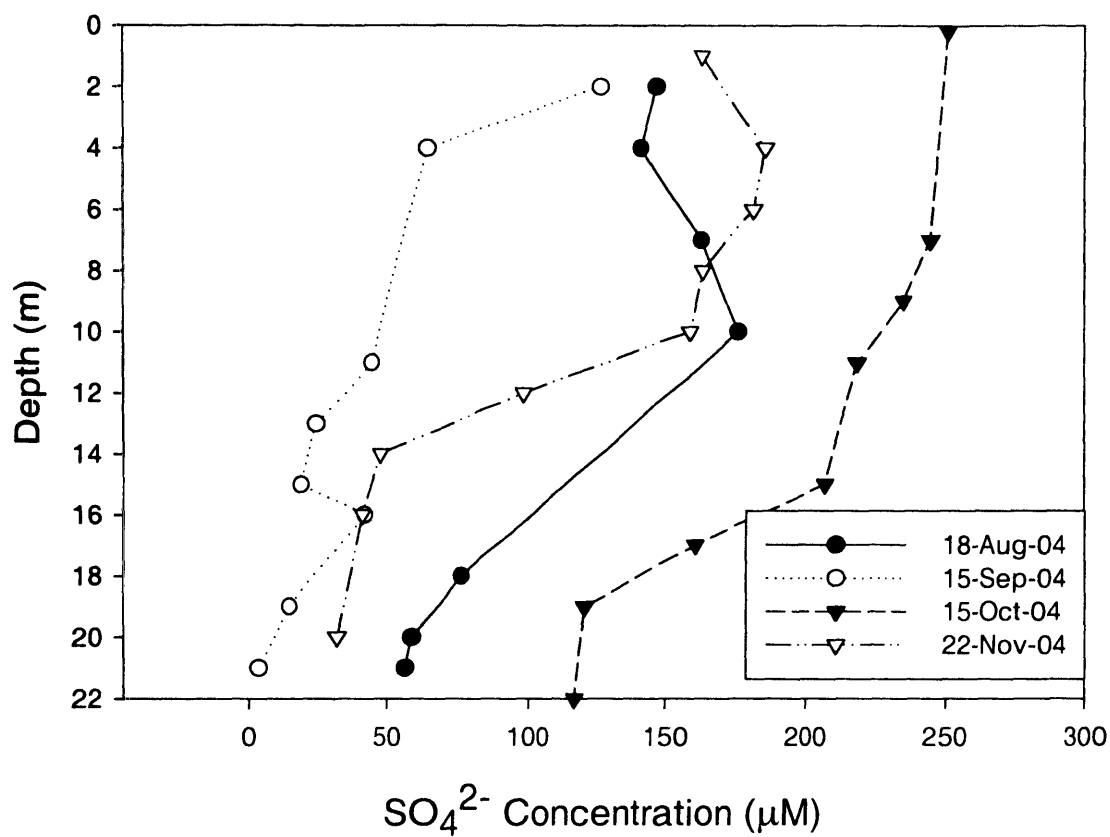


Table 3. Late September 2004 Storm Data

Site	Date	Time	Flow (m ³ /s)	SO ₄ ²⁻ (μM)	NH ₄ ⁺ (μM)	NO ₃ ⁻ (μM)
USGS*	9/28/2004	11:45	1.25	101.18	16.56	36.19
USGS*	9/28/2004	13:35	1.85	188.28	14.34	77.41
USGS*	9/28/2004	16:40	3.00	78.70	14.06	59.80
USGS*	9/28/2004	18:40	2.97	70.27	8.77	50.82
USGS*	9/29/2004	12:10	4.36	106.80	19.48	57.56
USGS*	9/30/2004	10:30	2.49	171.42	34.54	69.55
USGS*	10/1/2004	11:30	1.54	154.57	18.50	86.03

*USGS site located in the Aberjona River just upstream of UML (42.447° N, 71.138° W)

CH₄ and CO₂ Profiles

Dissolved methane distributions during the sampling period showed maximum concentrations at the sediments with a rapid decline towards a depth of ~10 m. The process of methanogenesis occurs in the sediments, during which organic matter is fermented into methane and carbon dioxide. Methane concentrations continued to increase throughout the sampling period and maximum concentrations of dissolved methane (705 μM) occurred on November 22, 2004. Concentrations in the epilimnion were always <1 μM . Figure 14 presents methane profiles from selected dates.

Due to atmospheric exchange, the epilimnion maintains a constant amount of CO₂. At the surface, the average CO₂ concentration was ~650 μM , which is about twice the amount expected if the surface water (using recorded pH data, Appendix B) were in equilibration with the atmosphere. The surface concentration was constant through the water column until ~10 m where it increased through the hypolimnion (Figure 15). The large amount of CO₂ in the hypolimnion is a result of the net decomposition of organic matter to CO₂ by the reactions described above.

Figure 14. CH₄ Profiles

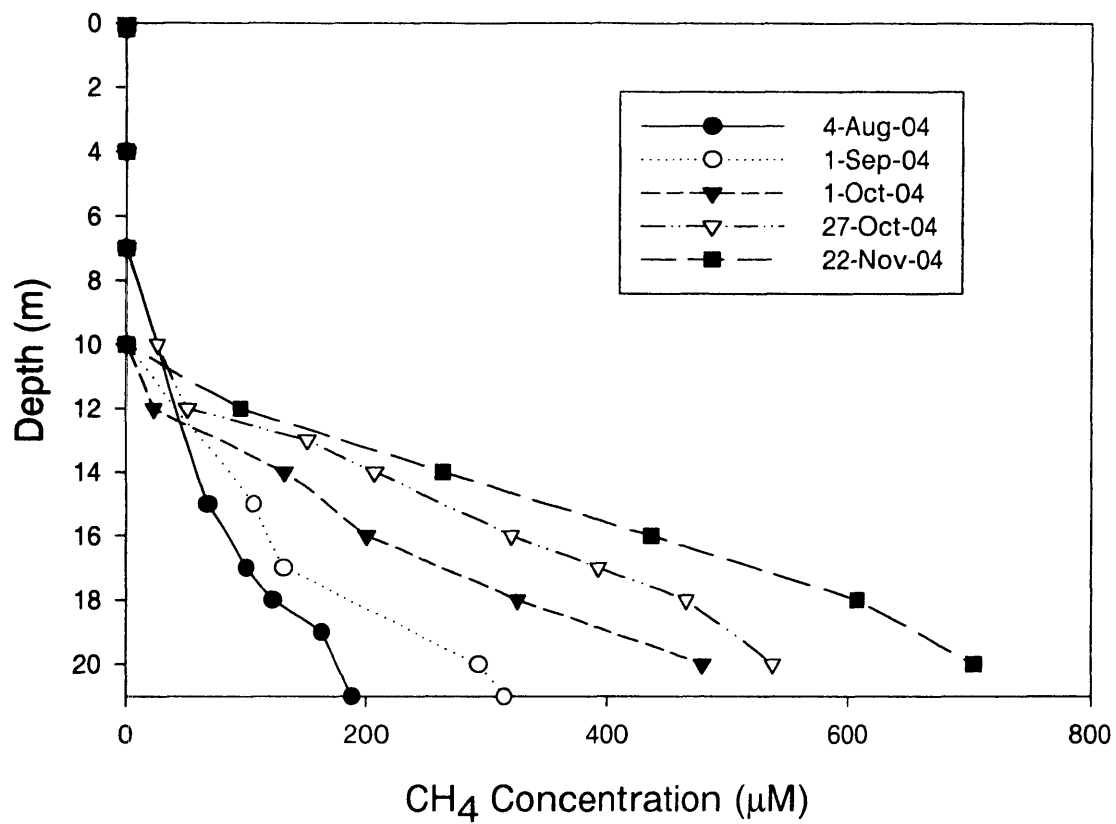
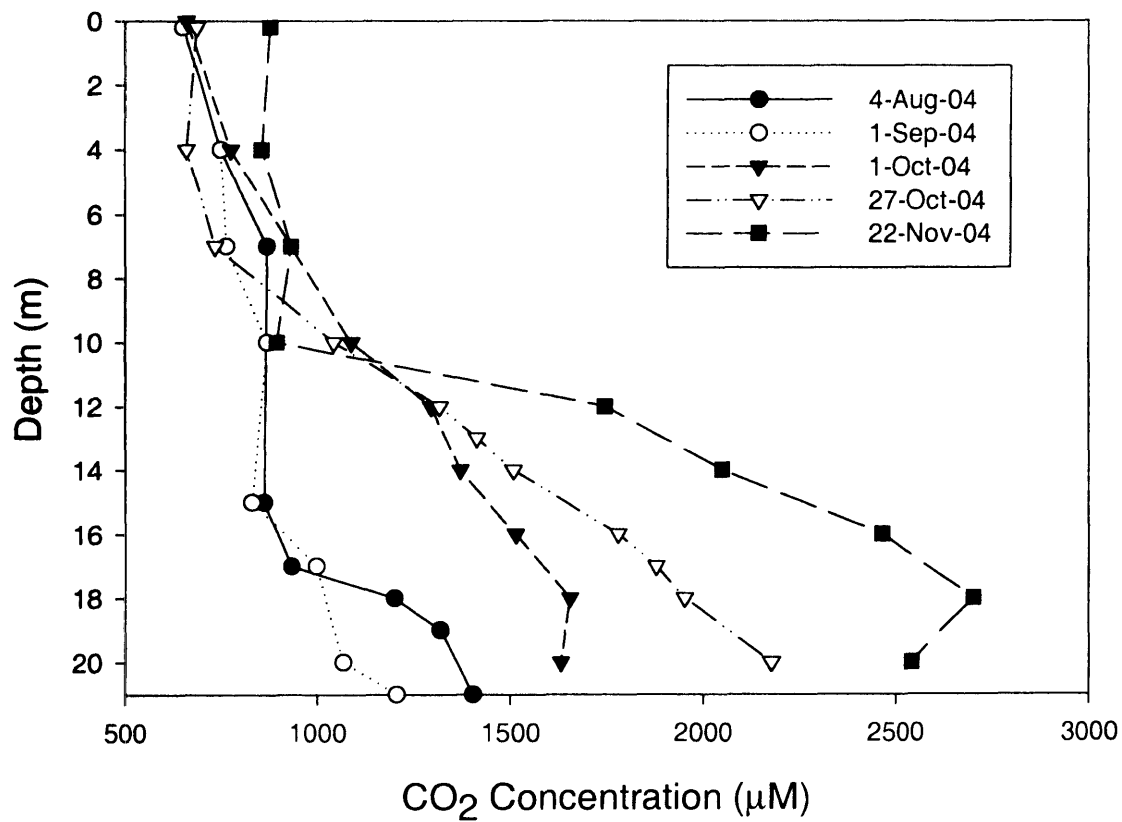


Figure 15. CO₂ Profiles



Rates of decomposition and reduction of electron acceptors

Changes in masses of CO₂ and CH₄ were linear with time indicating that the rate of decomposition of organic matter was constant throughout the measurement period (4-Aug-04 to 22-Nov-04; Figure 16). Similarly, changes in masses of the electron acceptors were also linear, except for SO₄²⁻ as mentioned above (Figure 17). In the case of SO₄²⁻ the rate of reduction was calculated for more than one time period (4-Aug-04 to 15-Sep-04 and 16-Sep-04 to 22-Nov-04). For the whole sampling period, molar quantities of methane and carbon dioxide changed the most, followed by sulfate and then iron (Table 4). Neither nitrate nor O₂ changed because measurements began after anoxia and nitrate depletion were established in UML.

The overall hypolimnetic decomposition rate, measured as CO₂ accumulation, was determined to be 7.5 ± 0.37 mmol CO₂ m⁻² d⁻¹. Unfortunately, there are no previous estimates of decomposition in UML to compare this value to. The hypolimnetic CO₂ accumulation rates determined by other studies are summarized in Table 5. Values in the range of 4.7 to 10.7 mmol CO₂ m⁻² d⁻¹, based on observations in other systems using similar hypolimnetic fractions, suggest that the model used here provides a reasonable rate estimate of organic matter decomposition in UML.

Figure16. Change in hypolimnetic mass of CO₂, CH₄ during 110 day sampling period

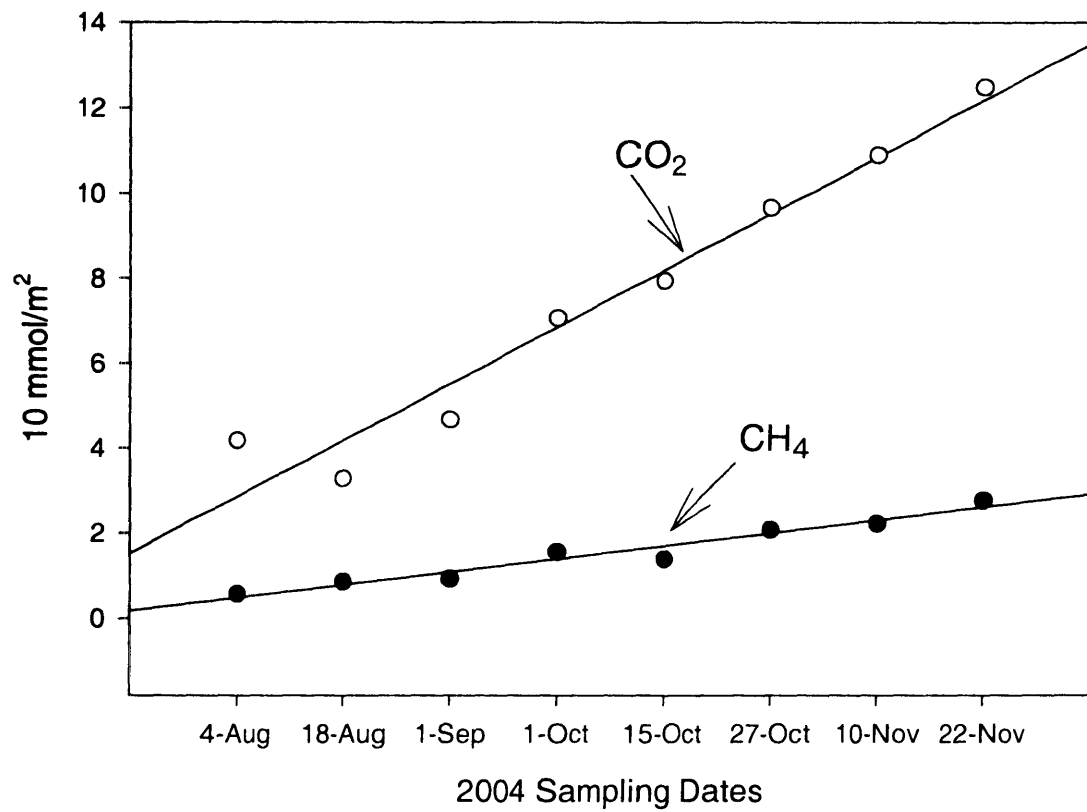


Figure 17. Change in hypolimnetic mass of O_2 , NO_3^- , Fe^{2+} and SO_4^{2-} during 110 day sampling period

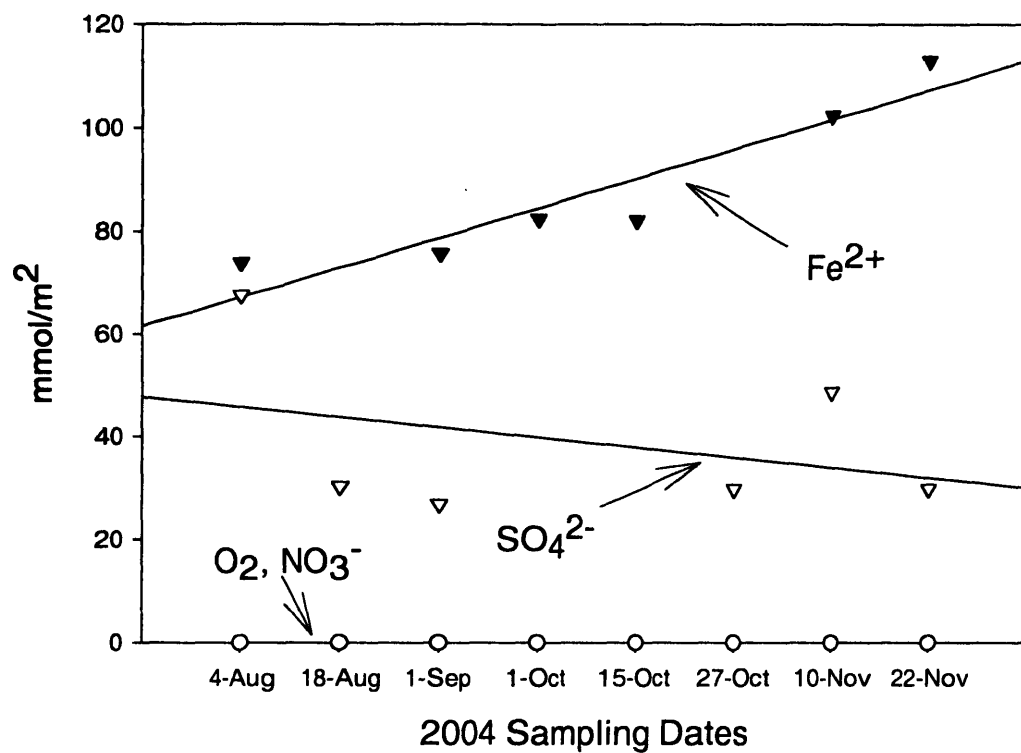


Table 4. Rates of change of hypolimnetic species

Species	Interval (no. of days)	Molar quantities $\text{mmol}\cdot\text{m}^{-2}\cdot\text{d}^{-1}$
O ₂	4 Aug – 22 Nov (110)	0
NO ₃ ⁻	4 Aug – 22 Nov (110)	0
Fe ²⁺	4 Aug – 22 Nov (110)	+0.36 ± 0.03
SO ₄ ²⁻	4 Aug - 15 Sep (42)	-1.35 ± 0.09
SO ₄ ²⁻	16 Sep - 22 Nov (68)	-0.71 ± 0.08
CH ₄	4 Aug – 22 Nov (110)	+1.99 ± 0.11
CO ₂	4 Aug – 22 Nov (110)	+7.54 ± 0.37

Table 5. Comparison of CO₂ accumulation in other lakes

Lake	CO ₂	Reference
	Accumulation mmol•m ⁻² •d ⁻¹	
L226N	8.1	Kelly et al. (1988)
L227	7.38	Kelly et al. (1988)
L223	7.62	Kelly et al. (1988)
Mirror	5.33	Mattson & Likens (1993)
Dart's	4.7	Schafran & Driscoll (1997)
UML	7.54	This Study

Uncertainty in rate estimates

Uncertainty estimates for the rates of decomposition and reduction of electron acceptors were calculated for the accumulation and diffusive flux terms. Accumulation uncertainty was determined by,

$$\Sigma (V \pm 10\%)_i \cdot ([S] \pm 10\%)_i \quad (5)$$

where *i* represents a stratum within the 15-20 m control volume (i.e. 15-16 m for the 15 m slice of the control volume) and *V* is the stratum volume, estimated from a best fit curve to UML bathymetric data with an associated uncertainty of $\pm 10\%$. The term, *S*, is a particular redox species concentration averaged from the top and bottom of that stratum. The analytical uncertainty in any laboratory measurement for a species concentration was determined using the method described by Miller and Miller (1984). All the standards measured during the experiment were used to construct a linear calibration curve. The standard deviation for the substance concentration was then calculated by *EXCEL* or *SigmaStat* statistical software and confidence limits for any measurement were calculated using a *t* value with *n*-2 degrees of freedom.

The turbulent diffusion term has an uncertainty calculated by

$$(K_z \pm 50\%) \cdot (d[S]/dz_{avg-15m} \pm s.d.) \cdot (A_{15m} \pm 10\%) \cdot \Delta t. \quad (6)$$

No uncertainty was used for the sampling period, Δt , because the maximum possible uncertainty (<12 hours = $\pm 3\%$) was insignificant relative to other errors. A_{15m} is the lake area at 15 m, which is equal to $1.85 \times 10^5 \text{ m}^2 \pm 10\%$. The term $d[S]/dz_{avg-15m} \pm s.d.$ is the average gradient over the sampling period at 15 m \pm the standard deviation of the gradient range. The vertical turbulent transport coefficient, K_z , as reported by Senn

(2001), was used as $0.02 \text{ cm}^2 \text{ s}^{-1} \pm 0.01$ (i.e. $\pm 50\%$) and is the majority of the uncertainty.

Total uncertainty for rates were calculated by standard methods of error propagation (Peters et al., 1974; Harris 1998).

Electron budget

The reducing equivalents were calculated based on the electrons necessary to reduce the molar quantities of electron acceptors. In the case of Fe^{2+} production 1 eq is used per mol Fe^{2+} produced. That is, one electron is needed to reduce Fe^{3+} to Fe^{2+} . Likewise, 8 electron equivalents are needed for sulfate reduction and methanogenesis. Therefore, the data in Table 6 represents an estimate of the electron flow through the anaerobic processes in the hypolimnion. The results of Table 6 indicate that the hypolimnetic electron budget was not balanced during the sampling period; the rate of CO_2 accumulation exceeded the combined rates of reduction of the electron acceptors. The electron balance showed an excess of 21 percent organic matter decomposition that was unexplained.

Table 6. Reducing equivalents necessary to reduce the molar quantities of electron acceptors

Species	Molar quantities $\text{mmol}\cdot\text{m}^{-2}$	Molar quantities $\text{mmol}\cdot\text{m}^{-2}\cdot\text{d}^{-1}$	Reducing equivalents $\text{mmol e}^{-}\cdot\text{m}^{-2}\cdot\text{d}^{-1}$
Fe^{2+}	39.13	0.36	0.36
SO_4^{2-}	-105.27	-0.96	7.66
CH_4	219.33	1.99	15.95
CO_2	829.50	7.54	30.16

Carbon Flow

The contribution of each electron acceptor to carbon flow (i.e. the complete breakdown of organic compounds to CO₂ and CH₄) is presented in Table 7. The associated carbon equivalents were estimated by assuming that the organic substrate contained the Redfield ratio of elements (i.e. glucose) and that it decomposed according to the stoichiometry shown in Table 1. In terms of carbon flow, methanogenesis was the predominant process, accounting for 53 percent of total organic matter decomposition during the sampling period. Sulfate reduction was the next most prevalent (25%) and then followed by iron, which accounted for 0.4 percent of total decomposition in UML.

Table 7. Carbon equivalents produced during the reduction of electron acceptors

Species	Molar quantities mmol·m⁻²	CO₂ equivalents Mmol C·m⁻²	% of CO₂ accumulation
Fe ²⁺	39 ± 3.3	3.3 ± 0.8	0.40
SO ₄ ²⁻	105 ± 10	210 ± 20	25.32
CH ₄	219 ± 12	439 ± 24	52.92
Excess CO₂ %			21.36

VI. DISCUSSION

Comparison to other lakes

There are other studies that have done relatively similar hypolimnetic budgets for redox active chemical species (Ingvorsen et al., 1982; Schafran and Driscoll, 1987; Kelly et al., 1988; Mattson and Likens, 1993). All of these studies used stoichiometric equations for the electron acceptors, analogous to those presented in Table 1, and carbohydrate type carbon as the carbon substrate. The overall electron budgets for the lakes examined in these studies varied from a 60 percent excess of electron acceptors in Lake 226N, Ontario, to a 37 percent excess of CO₂ in Mirror Lake, New Hampshire. The compiled data is summarized in Table 8.

The Canadian experimental lakes studied by Kelly et al. (1988) have little O₂ present in the hypolimnion and are therefore most comparable to UML. Like UML, the experimental lakes have the highest percentage of decomposition attributed to methane production; sulfate reduction also appears to be higher. Nitrate reduction is variable, but rather low, and iron reduction appears to be negligible in the CO₂ accumulation of the lakes, much like UML (Table 9).

Table 8. Comparison of overall electron budget from several lakes

Lake	Excess CO₂ %	Reference
L226N	-60	Kelly et al. (1988)
L227	-6	Kelly et al. (1988)
L223	11	Kelly et al. (1988)
Mirror	37	Mattson & Likens (1993)
Dart's	0	Schafran & Driscoll (1997)
UML	21	This Study

Table 9. Comparison of electron acceptors as percent of CO₂ accumulation to the Canadian experimental lakes

Lake	O₂	SO₄²⁻	NO₃⁻	CH₄	Fe	Total	Reference
Electron acceptor as percent of CO₂ accumulation							
L226N	47	25	13	71	3	160	Kelly et al. (1988)
L227	5.5	30	1	68	2	106	Kelly et al. (1988)
L223	9	30	1	42	6	88	Kelly et al. (1988)
UML	0	25	0	53	0.4	79	This study

Possible explanations for the electron imbalance

Possible explanations for the electron imbalance in UML fall into three categories: (1) calculation errors including analytical errors and errors in stoichiometry; (2) underestimation of iron reduction; and (3) underestimation of methane

Analytical errors were 10 percent or less for all the measured species. Even with an uncertainty of 20 percent, such analytical error is not likely to change the results of this study.

The overall stoichiometric ratios for the equations in Table 1 depend on the oxidation state of the carbon substrate. For example, the anaerobic degradation of cellulose theoretically yields equimolar amounts of CH_4 and CO_2 . If the carbon substrate was more reduced than carbohydrate, for instance a long-chain fatty acid, decomposition will yield a $\text{CH}_4:\text{CO}_2$ ratio greater than 1. Therefore, the amount of carbon flow during methanogenesis and other processes of organic matter mineralization depend on the chemical composition of the organic matter undergoing decomposition. The stoichiometric assumptions (Table 1) used in this study and by others (Kelly et al., 1988; Mattson and Likens, 1993) tend to overestimate the reduction rates. Correcting the equations using a carbon substrate with a lower oxidation state could lead to the reverse problem, a deficit of CO_2 with respect to that expected.

The rate of iron reduction may be underestimated by the method of measuring dissolved Fe^{2+} accumulation. It is likely that a certain amount of Fe^{2+} precipitates as FeS or FeS_2 minerals and is therefore being neglected in the budget. When anoxic conditions develop, Fe^{2+} that is produced can precipitate as FeS or FeS_2 , in the presence of enough sulfide (S^{2-}). Since this study only used dissolved Fe^{2+} accumulation as a measurement

of iron reduction, any iron reduction that resulted in FeS precipitation was neglected. In an attempt to correct for this problem, FeS formation was estimated by assuming: (1) that all of the reduced sulfate resulted in FeS formation and (2) that on a molar basis 30 percent of sulfate reduction resulted in formation of FeS (based on work by Rudd et al., 1986). Rudd et al. (1986) determined that an average of about one-third of the endproducts of sulfate reduction were iron sulfides which trap the iron in the sediments. After making these adjustments the excess CO₂ was reduced from 21 percent to 19 percent for the first case and to 20 percent excess CO₂ in the second. All in all, even maximum possible FeS formation does not explain the excess CO₂ accumulation in the hypolimnia of UML and concludes that iron reduction is small in terms of the total decomposition in UML.

There is also the possibility that methane production was underestimated and could account for the excess CO₂. Methane could have escaped from the sediments via ebullition and was therefore not measured by methane accumulation in the hypolimnion. Methane bubbles can form when the production of CH₄ within the sediments exceeds the rate of its removal. Consequently, the total gas pressures within the sediments exceeds the hydrostatic pressure; supersaturation and thus bubble formation occurs (Rudd and Taylor, 1980). Methane lost from the sediments by ebullition is lost from the aquatic environment entirely. By this way, the ecosystem loses energy, carbon and reducing equivalents, which affects the electron balance. In studies that have measured both methane accumulation in the water column and methane ebullition, the mass of methane lost via ebullition ranges from 8 percent to 50 percent of the total methane produced and is very lake specific (Rudd and Hamilton, 1978; Strayer and Tiedje, 1978; Fallon et al.,

1980; Mattson et al., 1993). To account for the excess CO₂ measured in this study, 0.78 mmol m⁻² d⁻¹ CH₄ would have been lost from the hypolimnion via ebullition, or 28 percent of the total CH₄ produced.

Finally, the underestimation of methane production and thus the budget discrepancy could be explained by the storage of methane (or another reduced product) in the sediments. The excess CO₂ accumulated at an average rate of about 1.6 mmol m⁻² d⁻¹ in UML throughout the sampling period. This rate of excess CO₂ accumulation could be explained by the accumulation of a reduced end product with a volume-weighted concentration of 35 μM (expressed as CO₂ equivalents) over a 110-day period. For example, if 4 liters of methane (at 0° C and 1 atmosphere pressure) were stored per m² of sediment in a 110-day period this would account for 100 percent of the excess CO₂. It is possible for methane to be stored in the sediments and diffuse out and be oxidized at other times of the year (Rudd and Hamilton, 1978).

VII. CONCLUSION

Decomposition of organic matter, measured by the accumulation rate of CO₂, was measured in the hypolimnion of UML. Rates of reduction of anoxic terminal electron acceptors were calculated but could not account for the decomposition of organic matter. During the period of this study approximately 80 percent of the decomposition in the hypolimnion of UML could be accounted for, while 20 percent remains unexplained. Several possibilities to explain the excess decomposition have been considered. The most likely possibility includes the underestimation of methane due to ebullition and/or the storage of gaseous methane in the sediments. Future studies in UML should include measurements of methane ebullition rates and iron sulfide particulates. Another useful measurement would be to determine the C:H:O ratio of organic matter in UML.

VIII. Appendix A

The Dissolved Gas Sampler

One of the main objectives of any water monitoring program involving fieldwork is the assurance of high quality, reliable data. In fact, the success of a water monitoring program can often depend on the sampling procedure adopted, regardless of how sophisticated the analytical approach may be. Unfortunately, sampling procedures have been neglected in recent years, while advancing analytical technology has been the focus (Broenkow 1969). It is important that an equal amount of effort should be directed towards improving and updating sampling methodology. This is particularly true for dissolved gases in hypolimnia of lakes since significant temperature and pressure changes can occur as the sample is lifted to the surface, as well as gas exchange with the atmosphere. The traditional method for sampling dissolved gases from the hypolimnion uses tubing and a peristaltic pump to fill glass BOD bottles at the surface. Such a method is not suitable for dissolved gases and introduces the possibility of all the problems mentioned above.

The problem of sampling dissolved gases from hypolimnia of lakes without outside influences (i.e. temperature changes, pressure changes and atmospheric contamination) required a portable sampler that could be used to obtain samples at precise depth intervals over the water column. The sampler described below was designed specifically to fit this need, but also allows samples to be analyzed by headspace equilibration without bottle transfer, maintains sampling depth pressure, and can be made for around ten dollars.

The sampler consists of a 45-cm-long polyvinyl chloride (PVC) housing frame that was sawed in half, long-wise. Onto the frame, 1.5" to 0.75" diameter PVC reducer bushings were affixed at each end using PVC cement. Two more bushings, sawed in

half, were cemented at each end and spaced apart to secure the lip of a 50 ml syringe in place. The syringes are held in place by the reducer bushings but can easily be attached or removed.

Before the syringes are attached to the PVC frame for sampling, the ~30 m tubing used to collect water samples for the other redox species is completely filled with water. Once this is done, the sampling syringe and the motor syringe (see Figure A-1 and A-2), which is completely filled with ~ 50 ml water, can be placed in the PVC frame. The motor syringe is then attached to one end of the tubing and the surface syringe (with no water) is attached to the other end of the tubing using tubing connectors. Because the motor syringe is filled with water, the plunger is fully extended and reaches the plunger end of the sampling syringe. The two plunger ends are connected using two Keck clamps; a Keck clamp happens to perfectly fit around the lip of a 50 ml syringe plunger. When the sampler is fully loaded and ready to lower over the side of the boat, the sampler is tied by a rope to the Hydrolab which serves as both a weight and depth meter.

As the sampler is lowered over the side of the boat, the 3-way Luer lok[®] valve on the sampler syringe is opened under water to eliminate air filling the valve. Once the sampler is lowered to the measuring depth, the 3-way Luer lok[®] valve on the surface syringe is opened. The plunger on the surface syringe is pulled and water from the tubing fills the surface syringe. As this is happening, the plunger on the motor syringe closes as water from the motor syringe replaces the water pulled from the tubing. Furthermore, since the motor and sampling syringes are connected end-to-end, the closing of the motor syringe plunger causes the sampling syringe plunger to open and fills the sampling

syringe with water. The amount of water pulled into the surface syringe is equal to the amount of water collected in the sampler syringe.

During sampling, the sampling syringe is flushed with water three times and is done so by simply pulling and closing the plunger of the surface syringe. After the desired sample volume is collected in the sampling syringe, the sampler and hydrolab are lifted to the surface and the 3-way Luer lok[®] valve on the sampling syringe is closed and capped underwater to avoid contact with the atmosphere. The sampling syringe is then removed from the PVC frame and immediately placed in a bucket of ice water. A new sampling syringe is placed into the PVC frame and the sampler is ready to be lowered to collect another sample.

It is important for the sample-filled syringes to be kept in cold water to avoid changes in sampling depth temperature and pressure. The ice water bucket used in this study was equipped with a “dock” of PVC reducer bushings cemented together (Figure A-3). This allowed the syringes to securely stand in the bucket with plunger up and not hit each other during transport.

Figure A-4 shows the water column profile of replicate samples of CO₂ taken on September 1, 2004. The replicate samples were on average within 6 percent of each other, indicating that the analytical method as well as sampling method used in this study afforded reliable dissolved gas data.

The dissolved gas sampler described above was used to obtain reliable samples at precise depth intervals while at the same time isolating the samples from outside influences. Moreover the sampler is easy to use and inexpensive to build. The sampler parts and costs are detailed in Table A-1. The total cost of the sampler, without syringes,

is estimated to be \$30.00, but most of the parts can be found around the lab and would not have to be purchased.

Figure A-1. The Dissolved Gas Sampler Diagram

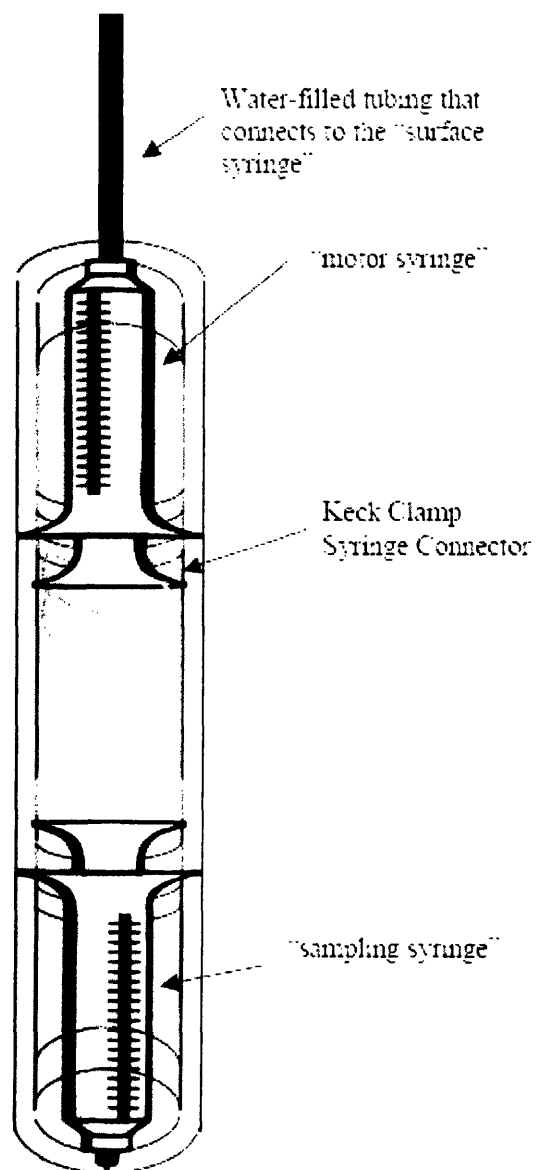


Figure A-2: The Dissolved Gas Sampler

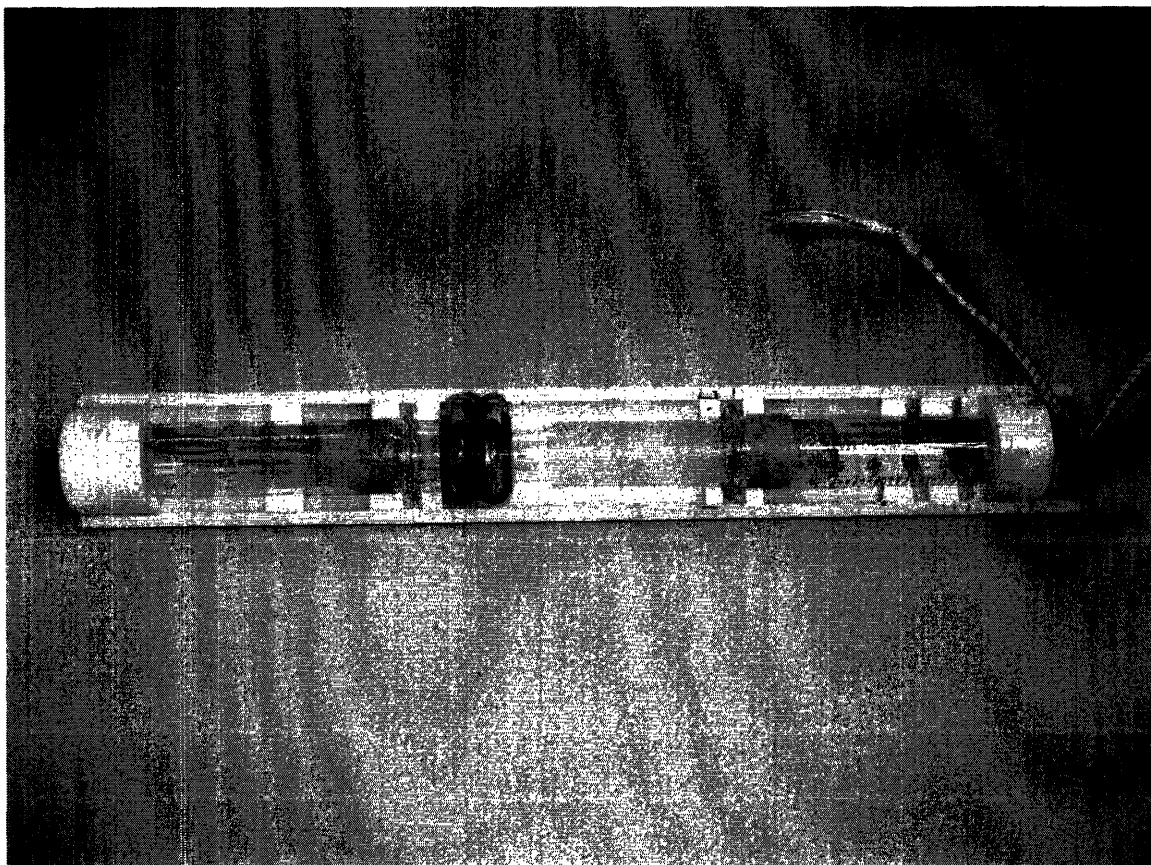


Figure A-3: Syringe “dock”

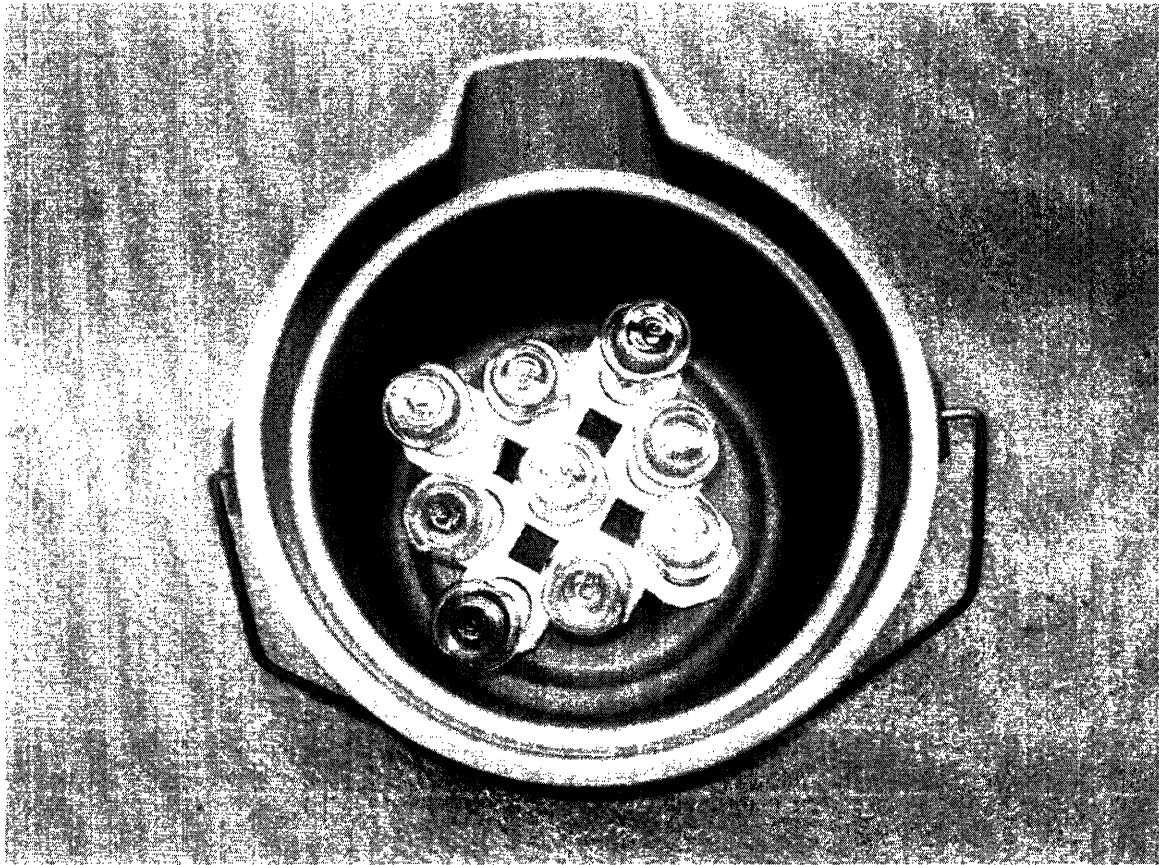


Table A-1. Cost and parts list for sampler

Part	#/ sampler	Cost	Cost/sampler
Tubing Connectors (1/8" Tubing)	3	14.77/20	\$2.21
3-way Luer lok valve	3	42.60/25	\$5.11
Tie wraps (6")	2	30.10/1000	\$0.06
Reducer Bushings (1.5" x 3/4" Slip)	8	0.95	\$7.60
PVC pipe (1.5")	1.47 ft	1.11/ft	\$1.63
Keck Clamp	2	24.00/6	\$8.00
Misc. hardware			\$5.50
PVC primer and cement			
Rope			
Total:			\$30.00

IX. Appendix B

Summary of Limnological Data

The hydrolab data and chemical species concentration profiles from the water column of the Upper Mystic Lake are tabulated on the following pages.

Table B-1. 13-May-04 Profile

Depth (m)	Temp (°C)	DO (mg/L)	pH
0.2	20.26	10.7	7.89
1	20.23	10.6	8.09
2	19.6	10.6	8.15
3	16.31	10.2	7.8
4	15.45	9.3	7.5
5	12.2	8.1	7.3
6	10.43	8.2	7.1
7	7.85	8.7	7.05
8	6.95	8.8	7
9	5.75	8.8	6.95
10	5.47	8.1	7.07
11	5.1	7.1	7
12	5.86	5.8	6.93
13	4.21	0.8	6.88
14	3.53	0.6	6.87
15	3.37	0.5	6.86
16	3.33	0.5	6.86

Table B-2. 27-May-04 Profile

Depth (m)	Temp (°C)	Cond (mS/cm)	DO (mg/L)	pH	ORP (mV)	NH₄⁺ (μM)	NO₃⁻ (μM)
0	16.63	0.71	8.44	7.47	548		
1	16.60	0.71	8.43	7.49	533	20.01	108.98
2	16.53	0.71	8.43	7.50	529		
3	16.44	0.71	8.32	7.50	524	13.31	73.58
4	15.93	0.67	8.10	7.47	514		
5	13.69	0.70	6.77	7.24	506	24.92	89.07
6	10.14	0.71	6.89	7.15	497		
7	7.90	0.75	7.40	7.09	467	43.32	108.98
8	6.73	0.78	7.56	7.06	415		
9	6.00	0.81	7.58	7.06	359		
10	5.61	0.86	6.77	7.04	332	55.01	100.13
11	5.28	0.91	6.00	7.04	309		
12	4.79	1.04	4.45	7.03	294	82.55	75.79
13	4.21	1.30	0.68	7.01	265		
14	3.85	1.46	0.45	7.03	225	119.72	40.39
15	3.63	1.53	0.37	7.03	211		
16	3.45	1.59	0.33	7.03	201		
18	3.32	1.68	0.29	7.03	181		
20	3.32	1.69	0.27	7.05	174		
22	3.35	1.53	0.26	7.08	166		
24	3.36	1.50	0.26	7.19	157		

Table B-3. 10-Jun-04 Profile

Depth (m)	Temp (°C)	DO (mg/L)	pH	ORP (mV)	NH₄⁺ (μM)	NO₃⁻ (μM)
0.2	20.77	8.85	5.58	549	13.56	146.11
1	21.36	9.38	6.1	532		
2	21.68	9.32	7	486		
3	20.6	9.41	6.9	497		
4	20.54	8.92	6.83	504	22.67	141.45
5	20.3	7.81	6.78	508		
6	18	5.75	6.35	519		
7	16.41	5.15	6.19	524		
8	14.64	4.99	6.06	527	36.39	138.33
9	8.05	6.83	5.61	533		
10	7	6.9	6.5	510		
11	5.69	4.94	6.9	456	61.92	118.10
12	5.09	3.22	6.91	337		
13	4.6	0.8	6.91	314	131.23	26.26
14	4.2	0.26	6.87	171		
15	3.93	0.23	6.86	154	221.39	0.00
16	3.74	0.24	6.86	152		
17	3.51	0.24	6.85	148		
18	3.39	0.24	6.9	137	231.99	0.00
19	3.39	0.26	6.9	134		
20	3.39	0.24	6.91	130	208.20	0.00
21	3.38	0.22	6.92	125		
22	3.39	0.22	6.98	121	237.14	0.00

Table B-4. 23-Jun-04 Profile

Depth (m)	Temp (°C)	Cond (mS/cm)	DO (mg/L)	pH	ORP (mV)	Fe²⁺ (μM)	NH₄⁺ (μM)	NO₃⁻ (μM)
0.2	22.01	0.72	8.2	7.54	513		10.84	144.56
1	22.01	0.72	8.34	7.68	514			
2	21.94	0.72	8.39	7.71	514		11.07	138.33
3	21.89	0.72	8.15	7.73	510			
4	20.45	0.71	7.83	7.47	509		29.64	138.33
5	15.22	0.71	5.42	7.1	510			
6	12.35	0.73	4.83	6.87	510			
7	8.76	0.77	4.95	6.77	500		29.85	132.11
8	7.37	0.80	4.87	6.65	430			
9	6.29	0.84	4.31	6.62	371			
10	5.81	0.89	3.57	6.63	329			
11	5.33	0.96	2.96	6.67	319			
12	4.63	1.19	1.2	6.7	295			
13	4.16	1.42	0.36	6.78	267		144.87	4.47
14	3.88	1.53	0.26	6.79	245			
15	3.71	1.59	0.25	6.79	240	8.20	214.27	0.00
16	3.59	1.63	0.23	6.79	230			
17	3.47	1.68	0.22	6.79	224	31.48	212.90	0.00
18	3.41	1.73	0.21	6.8	213			
19	3.4	1.74	0.22	6.83	210	64.81	233.36	0.00
20	3.38	1.75	0.19	6.85	193	71.76	253.66	0.00
21	3.39	1.75	0.18	6.87	186			
22	3.4	1.75	0.19	6.89	184	80.77	246.31	0.00

Table B-5. 7-Jul-04 Profile

Depth (m)	Temp (°C)	Cond (mS/cm)	DO (mg/L)	pH	ORP (mV)	Fe²⁺ (μM)	NH₄⁺ (μM)	NO₃⁻ (μM)
0.2	24.75	0.72	8.37	7.74	390			
1	24.66	0.72	8.4	7.78	389			
2	24.5	0.72	8.42	7.79	389		10.93	79.12
3	24.47	0.71	8.35	7.8	389			
4	21.05	0.71	7.42	7.32	384		9.82	81.65
5	16.34	0.72	5.63	6.96	365			
6	11.24	0.76	3.3	6.65	321			
7	8.76	0.79	3.23	6.43	267		20.93	75.32
8	7.25	0.82	3.3	6.41	235			
9	6.18	0.87	2.44	6.38	211			
10	5.73	0.92	1.52	6.39	198			
11	5.14	1.02	1.12	6.43	175			
12	4.76	1.14	0.54	6.44	158			
13	4.2	1.43	0.38	6.49	142		141.01	8.22
14	4.04	1.50	0.54	6.53	51			
15	3.8	1.59	0.43	6.52	37	54.84	148.71	8.22
16	3.57	1.67	0.32	6.57	19			
17	3.48	1.73	0.34	6.58	14	54.03	160.77	0.00
18	3.45	1.74	0.52	6.63	36			
19	3.44	1.76	0.45	6.63	29	53.25	157.39	0.00
20	3.46	1.77	0.4	6.65	23			
21	3.46	1.78	0.37	6.68	17	107.49	188.54	0.00

Figure B-6. 21-Jul-04 Profile

Depth (m)	Temp (°C)	Cond (mS/cm)	DO (mg/L)	pH	ORP (mV)	Fe²⁺ (μM)	NH₄⁺ (μM)	NO₃⁻ (μM)	SO₄²⁻ (μM)
0.4	25	0.61	9.2	8	179		15.99	79.12	195.98
1	25	0.61	8.98	8.08	180				
2	24.91	0.61	8.63	8.1	181		29.89	104.44	223.25
3	23.64	0.61	8.9	7.9	184				
4	22.48	0.60	7.58	7.26	189		22.08	152.55	234.48
5	17.79	0.63	4.68	6.53	199				
6	13.63	0.64	1.77	6.19	207				
7	9.6	0.68	2.07	6.03	213		44.81	6.95	249.72
8	7.64	0.71	2.06	5.96	216				
9	6.56	0.75	0.85	5.92	219				
10	6.02	0.78	0.37	5.9	221				
11	5.53	0.86	0.17	5.92	223				
12	4.93	1.00	0.06	5.99	214				
13	4.44	1.18	0.03	6.03	193		149.14	0.00	206.41
14	4.08	1.32	0	6.03	192				
15	3.77	1.40	0	6.04	37	33.24	174.51	0.00	214.43
16	3.6	1.45	0	6.06	16	63.89	195.58	0.00	
17	3.52	1.49	0	6.1	2				
18	3.5	1.51	0	6.14	-17	111.50	199.26	0.00	190.36
19	3.47	1.52	0	6.19	-33	116.73	217.98	0.00	146.25
20	3.48	1.53	0	6.23	-41				
21	3.5	1.54	0	6.29	-50	184.93			174.32

Table B-7. 4-Aug-04 Profile

Depth (m)	Temp (°C)	Cond (mS/cm)	DO (mg/L)	pH	ORP (mV)	Fe²⁺ (μM)
0.3	26.36	0.48	10.36	8.67	154	
1	26.37	0.48	10.35	8.68	156	
2	26.36	0.48	10.35	8.69	158	
3	24.5	0.48	9.54	7.44	168	
4	21.77	0.46	4.03	6.57	186	
5	18.37	0.60	2.01	6.36	200	
6	13.89	0.65	0.36	6.09	207	
7	10.15	0.67	0.5	5.95	210	
8	7.34	0.71	1.29	5.89	214	
9	6.6	0.75	0.28	5.89	216	
10	5.84	0.79	0.1	5.87	217	
11	5.37	0.84	0	5.9	213	
12	4.88	0.98	0	5.99	208	
13	4.45	1.09	0	6.04	198	
14	4.08	1.29	0	6.05	189	
15	3.79	1.39	0	6.08	51	59.05
16	3.55	1.49	0	6.16	-10	148.48
17	3.51	1.51	0	6.21	-36	
18	3.5	1.52	0	6.29	-73	158.80
19	3.51	1.53	0	6.33	-89	189.24
20	3.52	1.53	0	6.37	-102	
21	3.53	1.53	0	6.4	-113	

Table B-8. 4-Aug-04 Profile continued

Depth (m)	NH₄⁺ (μM)	NO₃⁻ (μM)	SO₄²⁻ (μM)	CO₂ (μM)	CH₄ (μM)
0.3					
1					
2	30.42	48.16	182.65		
3					
4	29.33	55.84			
5					
6					
7					
8					
9					
10	84.31	11.29	179.10		
11					
12					
13	123.76	9.75	170.21		
14					
15	146.58	8.21	170.21	860.44	67.64
16					
17	137.48	9.75	169.33	931.96	99.69
18	159.47	9.75	152.45	1202.04	122.57
19	173.25	9.75	86.73	1319.35	161.12
20					
21				1404.12	188.42

Table B-9. 18-Aug-04 Profile

Depth (m)	Temp (°C)	Cond (mS/cm)	DO (mg/L)	pH	ORP (mV)	Fe²⁺ (μM)
0.2	23.43	0.50	7.4	7.44	536	
1	23.32	0.50	7.16	7.65	537	
2	22.83	0.49	6.93	7.65	536	
3	22.52	0.50	6.45	7.54	535	
4	21.5	0.49	3.5	7.09	534	
5	19.42	0.63	0.71	6.84	535	
6	15.01	0.77	0.48	6.7	535	
7	9.92	0.82	0.62	6.55	521	
8	8.11	0.85	1.18	6.54	499	
9	6.55	0.92	0.61	6.53	478	
10	5.8	0.97	0.6	6.56	464	
11	5.41	1.02	0.6	6.62	450	
12	4.9	1.18	0.61	6.69	440	
13	4.58	1.33	0.62	6.75	431	
14	4.16	1.56	0.63	6.79	422	
15	3.76	1.73	0.63	6.81	413	50.07
16	3.64	1.80	0.64	6.85	402	
17	3.57	1.84	0.64	6.92	390	96.42
18	3.54	1.80	0.65	6.98	376	167.69
19	3.54	1.86	0.65	7.02	364	
20	3.55	1.86	0.65	7.06	355	246.87
21	3.57	1.88	0.65	7.09	334	236.54

Table B-10. 18-Aug-04 Profile continued

Depth (m)	NH ₄ ⁺ (μM)	NO ₃ ⁻ (μM)	SO ₄ ²⁻ (μM)	CO ₂ (μM)	CH ₄ (μM)
0.2				649.815	1.89
1					
2	31.39	40.48	146.71		
3					
4	39.50	38.94	141.08		
5					
6					
7	5.72	115.75	162.20		
8					
9					
10	11.77	126.50	176.28		
11					
12	69.97	31.26			
13					
14					
15				458.40	116.98
16					
17				731.86	128.53
18	214.38	11.29	76.33	619.98	200.00
19					
20	221.77	12.06	58.73	844.37	261.04
21	416.10	9.75	56.62	658.90	199.95

Table B-11. 1-Sep-04 Profile

Depth (m)	Temp (°C)	Cond (mS/cm)	DO (mg/L)	pH	ORP (mV)	Fe ²⁺ (μM)
0.3	24.83	0.52	7.8	7.72	574	
1	24.83	0.52	7.8	7.9	572	
2	24.82	0.52	7.77	7.96	569	
3	24.8	0.52	7.59	8.03	567	
4	21.88	0.52	2.94	7.25	560	
5	19.98	0.55	0.5	7.11	556	
6	14.5	0.79	0.45	6.98	553	
7	10.56	0.83	0.44	6.9	534	
8	8.9	0.86	0.55	6.85	496	
9	6.77	0.93	0.49	6.86	486	
10	5.96	0.99	0.49	6.88	468	
11	5.23	1.12	0.48	6.92	465	
12	4.91	1.23	0.48	6.97	453	
13	4.52	1.43	0.5	7.02	443	
14	4.16	1.62	0.51	7.05	435	
15	3.87	1.71	0.5	7.09	422	109.63
16	3.74	1.80	0.51	7.11	413	
17	3.7	1.83	0.51	7.13	403	167.08
18	3.65	1.85	0.51	7.17	394	
19	3.61	1.88	0.51	7.2	384	132.41
20	3.6	1.89	0.52	7.21	376	221.50
21	3.6	1.88	0.52	7.22	368	218.99

Table B-12. 1-Sep-04 Profile continued

Depth (m)	NH ₄ ⁺ (μM)	NO ₃ ⁻ (μM)	SO ₄ ²⁻ (μM)	CO ₂ (μM)	CH ₄ (μM)
0.3	0.89	0.00	87.49	649.82	0.74
1					
2	10.43	21.27	112.76		
3					
4	17.87	25.11	118.51		
5					
6	16.90	28.19	152.97		
7					
8	19.97	52.76	43.84		
9					
10	59.25	29.72	78.30		
11					
12					
13	112.78	22.04	95.53		
14					
15	150.93	8.98	69.11	866.53	146.67
16					
17				829.82	120.40
18					
19	168.29	0.00	78.30	998.22	235.55
20				1067.50	317.67
21			38.09	1207.52	229.20

Table B-13. 15-Sep-04 Profile

Depth (m)	Temp (°C)	Cond (mS/cm)	DO (mg/L)	pH	ORP (mV)	Fe ²⁺ (μM)
0.2	21.48	0.54	8.18	7.74	555	
1	21.54	0.54	8.5	9.02	544	
2	21.53	0.54	8.19	8.04	541	
3	21.53	0.54	8.23	8.06	536	
4	21.53	0.54	8.5	9.04	533	
5	20.6	0.56	4.64	7.25	529	
6	15.85	0.78	2.4	6.9	523	
7	11.49	0.84	2.15	6.74	517	
8	9.37	0.86	1.97	6.67	512	
9	7.25	0.93	1.92	6.62	505	
10	6.16	1.00	1.55	6.63	493	
11	5.55	1.06	1.34	6.71	481	
12	4.88	1.26	1.22	6.78	478	
13	4.6	1.42	1.08	6.85	464	
14	4.14	1.67	1	6.88	457	
15	3.92	1.76	0.97	6.91	445	66.07
16	3.77	1.83	0.98	6.95	428	
17	3.71	1.86	0.8	7.01	412	115.89
18	3.67	1.88	0.76	7.05	393	
19	3.62	1.91	0.71	7.1	372	172.95
20	3.63	1.92	0.67	7.13	357	183.73
21	3.64	1.92	0.64	7.17	345	205.04

Table B-14. 15-Sep-04 Profile continued

Depth (m)	NH₄⁺ (μM)	NO₃⁻ (μM)	SO₄²⁻ (μM)	CO₂ (μM)	CH₄ (μM)
0.2				649.81	0.00
1					
2	0.93	36.58	125.81		
3					
4	21.56	42.07	63.64		
5					
6					
7	104.77	75.01	170.21		
8					
9					
10					
11	106.93	5.01	44.10		
12					
13			24.56	650.66	28.59
14					
15	149.46	0.00	19.23	668.02	47.97
16	214.02	0.00	41.44		
17				704.43	21.27
18					
19	437.11	0.00	1.47	839.11	179.96
20					
21			3.25	799.41	193.62

Table B-15. 1-Oct-04 Profile

Depth (m)	Temp (°C)	Cond (mS/cm)	DO (mg/L)	pH	ORP (mV)	Fe ²⁺ (μM)
0.2	18.76	0.42	9.41	7.94	483	
1	18.55	0.42	9.34	7.55	495	
2	18.33	0.42	9.23	7.37	499	
3	18.1	0.42	8.96	7.16	500	
4	17.4	0.41	6.82	6.62	513	
5	17.1	0.41	5.57	6.38	516	
6	15.8	0.45	4.25	6.35	519	
7	13.9	0.63	0.65	6.35	534	
8	9.17	0.70	0.47	6.37	555	
9	7.6	0.73	0.45	6.21	562	0.00
10	6.5	0.77	0.5	6.06	561	
11	5.7	0.82	0.39	6.12	558	0.00
12	5.1	0.96	0.38	7.06	4.88	
13	4.5	1.15	0.4	7.1	493	0.65
14	4.2	1.28	0.34	7.16	421	
15	3.9	1.41	0.35	7.31	296	79.30
16	3.7	1.45	0.38	7.45	281	
17	3.6	1.48	0.33	7.6	253	174.23
18	3.6	1.51	0.4	7.7	241	
19	3.6	1.51	0.42	7.75	236	216.28
20	3.6	1.51	0.37	7.8	228	
21	3.6	1.52	0.33	7.6	221	
21.5	3.6	1.52	0.35	7.95	208	

Table B-16. 1-Oct-04 Profile continued

Depth (m)	NH₄⁺ (μM)	NO₃⁻ (μM)	SO₄²⁻ (μM)	CO₂ (μM)	CH₄ (μM)	P (μg/L)
0.2	14.42	48.93	113.58	354.22	0.00	
1						
2	16.58	51.68	156.75			10.32
3						
4	42.75	53.05	142.36	416.28	0.00	11.38
5						
6						3.29
7	24.28	85.99	198.49			
8						
9	30.00	107.95	149.56			
10				1087.99	0.00	
11	59.72	83.25	185.53			10.12
12				1294.67	15.41	
13	257.95	7.76	250.3			8.02
14				1370.23	89.00	
15	389.39	0.00	185.53			15.76
16				1513.18	135.42	22.15
17	434.51	0.00	153.15			
18				1655.0	220.29	22.44
19	493.81	0.00	203.52			22.71
20				1630.84	324.33	
21						38.74
21.5						

Table B-17. 15-Oct-04 Profile

Depth (m)	Temp (°C)	Cond (mS/cm)	DO (mg/L)	Fe²⁺ (μM)
0.2	15.17	0.48	9.03	
1	15.13	0.48	8.5	
2	15.09	0.48	8.77	
3	15.04	0.49	8.4	
4	15.02	0.49	8.26	
5	14.85	0.49	7.74	
6	14.62	0.52	5.93	
7	11.04	0.74	0.37	
8	8.00	0.80	0.37	
9	6.76	0.85	0.39	
10	5.83	0.89	0.41	
11	5.35	0.98	0.43	0.00
12	4.66	1.18	0.45	
13	4.35	1.35	0.45	10.19
14	4.07	1.47	0.49	
15	3.8	1.58	0.52	75.87
16	3.69	1.63	0.61	
17	3.64	1.66	0.54	164.51
18	3.63	1.67	0.54	
19	3.64	1.68	0.59	226.74
20	3.65	1.68	0.59	
21	3.65	1.68	0.61	
22	3.67	1.69	0.78	264.26

*no pH and ORP data, sensors were not functioning properly

Table B-18. 15-Oct-04 Profile continued

Depth (m)	NH₄⁺ (μM)	NO₃⁻ (μM)	SO₄²⁻ (μM)	CO₂ (μM)	CH₄ (μM)	P (μg/L)
0.2	13.84	57.17	250.3	105.54	0	11.84
1						
2						
3						
4	26.19	80.50	189.85	676.19	0	8.70
5						
6						
7	41.60	92.85	422.24	785.39	0	18.94
8						
9	79.35	87.36	235.19			21.84
10				934.85	0	
11	182.58	39.33	217.92			25.37
12				1016.99	69.98	
13	388.26	0.00	181.94	1360.33	105.12	13.76
14						
15	427.21	0.00	207.12	1372.19	160.03	38.44
16						
17	471.91	0.00	160.35	1564.68	164.86	23.22
18						
19	503.07	0.00	120.77	1741.56	180.47	19.99
20				1743.32	212.63	
21						
22	651.00	0.00	117.17	1684.78	247.92	37.39

Table B-19. 27-Oct-04 Profile

Depth (m)	Temp (°C)	Cond (mS/cm)	DO (mg/L)	pH	ORP (mV)	Fe²⁺ (μM)
0.2	11.54	0.52	9.47	8.36	403	
1	11.53	0.52	9.67	8.25	406	
2	11.47	0.52	9.36	7.63	443	
3	11.46	0.53	9.36	7.64	440	
4	11.45	0.53	9.33	7.68	432	
5	11.45	0.53	9.34	8.37	526	
6	11.43	0.53	9.28	7.93	402	
7	11.39	0.53	8.83	8.05	373	
8	9.57	0.68	4.1	7.77	333	
9	6.54	0.85	0.29	6.71	344	
10	5.83	0.90	0.36	6.36	354	0.00
11	5.44	0.96	0.37	6.32	350	
12	4.86	1.12	0.41	6.41	318	2.65
13	4.39	1.33	0.55	6.82	275	
14	4.05	1.48	0.41	6.36	287	38.50
15	3.8	1.57	0.45	6.5	267	
16	3.72	1.61	0.45	6.56	267	311.18
17	3.68	1.63	0.42	6.57	265	
18	3.66	1.64	0.47	6.55	283	305.75
19	3.67	1.65	0.47	6.67	280	
20	3.78	1.60	0.52	6.81	308	263.87

Figure B-20. 27-Oct-04 Profile continued

Depth (m)	NH₄⁺ (μM)	NO₃⁻ (μM)	SO₄²⁻ (μM)	CO₂ (μM)	CH₄ (μM)	P (μg/L)
0.2			44.40	684.45	0.00	
1	10.46	22.60				12.85
2						
3	13.95	65.17	64.52			13.83
4				658.44	0.00	
5						
6	15.93	48.14	126.54			1.87
7				733.66	0.00	
8	22.53	93.54	192.75			8.75
9						
10	42.38	90.71	136.60	1042.80	17.28	2.13
11						
12	119.47	31.11	184.37	1316.46	35.02	4.36
13				1413.30	99.93	
14	102.59	0.00	30.99	1506.62	138.66	19.66
15						
16	293.08	0.00	83.80	1777.17	215.20	20.45
17				1878.78	312.63	
18	287.59	0.00	141.63	1952.92	361.38	23.13
19						
20	374.47	0.00	72.90	2177.91	263.71	42.02

Table B-21. 10-Nov-04 Profile

Depth (m)	Temp (°C)	Cond (mS/cm)	DO (mg/L)	pH	Fe ²⁺ (μM)
0.2	9	0.593	9.31	7.53	
1	9.01	0.594	9.29	7.55	
2	8.93	0.594	9.12	7.53	
3	8.8	0.593	8.5	7.52	
4	8.78	0.592	8.51	7.53	
5	8.77	0.592	8.36	7.56	
6	8.75	0.591	8.62	7.59	
7	8.73	0.59	8.66	7.61	
8	8.68	0.59	8.78	7.64	
9	8.7	0.588	8.13	7.56	
10	8.14	0.514	2.26	7.87	0.00
11	6.16	0.587	0.17	7.38	
12	5.12	0.688	0.18	7.66	0.00
13	4.74	0.795	0.19	7.77	
14	4.31	0.898	0.21	7.97	25.04
15	4.04	0.947	0.21	8.01	
16	3.89	1.572	0.21	8.03	120.61
17	3.8	1.607	0.21	8.06	
18	3.77	1.646	0.24	8.03	214.97
19	3.76	1.655	0.23	7.98	
20	3.81	1.654	0.29	7.8	306.39

*ORP sensor not functioning properly

Table B-22. 10-Nov-04 Profile continued

Depth (m)	NH ₄ ⁺ (μM)	NO ₃ ⁻ (μM)	SO ₄ ²⁻ (μM)	CO ₂ (μM)	CH ₄ (μM)	P (μg/L)
0.2				649.70	0.00	
1	13.76	48.14	109.50			
2						2.36
3						
4	16.27	73.68	150.42	775.82	0.00	2.08
5						
6	15.69	76.52	149.98			1.81
7				805.93	0.00	
8	16.05	79.36	146.02			2.19
9				814.11	0.00	
10	104.41	42.46	141.18	1208.95	0.00	3.00
11						
12		16.92	75.19	1442.66	5.70	4.14
13						
14	280.71	0.00	54.08	1847.86	122.68	3.66
15				2182.96	252.42	
16	300.65	0.00	106.43	1911.28	184.61	8.00
17						
18	305.88	0.00	102.03	2297.64	374.18	18.04
19						
20	366.48	0.00	79.59	2251.26	327.65	36.31

Table B-23. 22-Nov-04 Profile

Depth (m)	Temp (°C)	Cond (mS/cm)	DO (mg/L)	pH	Fe ²⁺ (μM)
0.2	7.1	0.637	11.62	7.57	
1	7.09	0.637	11.4	7.58	
2	7.09	0.637	10.41	7.6	
3	7.08	0.637	10.65	7.6	
4	7.05	0.417	11.06	7.62	
5	7.03	0.417	11.01	7.62	
6	6.94	0.419	10.51	7.62	
7	6.72	0.435	9.83	7.56	
8	6.67	0.446	10.23	7.59	
9	6.4	0.45	9.42	7.59	
10	6.12	0.5	8.2	7.58	
11	5.86	0.592	2.32	7.41	
12	5.48	0.68	0.19	7.64	0.00
13	4.67	0.857	0.21	7.82	
14	4.28	0.928	0.21	7.99	26.09
15	4.12	0.967	0.22	8.04	
16	3.95	0.997	0.25	8.14	94.87
17	3.83	1.029	0.25	8.24	
18	3.79	1.043	0.33	8.26	268.70
19	3.8	1.049	0.43	8.25	
20	3.81	1.052	0.63	7.77	353.02

Table B-25. 22-Nov-04 Profile continued

Depth (m)	NH ₄ ⁺ (μM)	NO ₃ ⁻ (μM)	SO ₄ ²⁻ (μM)	CO ₂ (μM)	CH ₄ (μM)	P (μg/L)
0.2				874.85	0.00	
1	15.43	65.96	162.29			1.44
2						
3						
4	21.05	65.96	181.21	853.07	0.00	1.22
5						
6	9.96	33.68	98.07			1.01
7				929.68	0.00	
8	21.42	68.11	185.17			1.12
9						
10	16.87	10.01	47.48	892.50	0.00	1.53
11						
12	67.50	16.46	162.73	1742.82	62.15	2.46
13						
14	190.24	0.00	158.33	2048.56	179.49	1.54
15						
16		0.00	40.44	2462.34	298.75	11.47
17						
18	188.57	0.00	110.38	2703.48	433.67	20.81
19						
20		0.00	31.64	2543.25	486.36	36.23

Table B-26. 15-Dec-04 Profile

Depth (m)	Temp (°C)	Cond (mS/cm)	DO (mg/L)	pH	Fe²⁺ (μM)
0.2	4.67	0.645	10.39	8.15	
1	4.67	0.644	10.35	8.31	
2	4.69	0.645	10.33	8.19	
3	4.69	0.645	10.22	8.16	
4	4.69	0.645	10.33	8.13	
5	4.67	0.645	10.38	8.12	
6	4.71	0.645	10.46	8.11	
7	4.71	0.645	10.21	8.07	
8	4.71	0.645	10.36	8.06	
9	4.71	0.645	10.37	8.04	
10	4.76	0.646	10.3	8.02	0.00
11	4.75	0.646	10.18	7.99	
12	4.75	0.646	10.15	8	0.00
13	4.88	1.323	0.62	7.63	
14	4.46	1.434	0.5	7.56	0.21
15	4.24	1.507	0.4	7.65	
16	3.94	1.614	0.36	7.82	4.24
17	3.85	1.661	0.3	7.98	
18	3.85	1.672	0.29	8.11	51.95
19	3.85	1.678	0.27	8.22	
20	3.85	1.686	0.26	8.2	189.56

Table B-27. 15-Dec-04 Profile continued

Depth (m)	NH ₄ ⁺ (μM)	NO ₃ ⁻ (μM)	SO ₄ ²⁻ (μM)	CO ₂ (μM)	CH ₄ (μM)
0.2				926.42	0.00
1					
2					
3					
4					
5					
6					
7	24.60	51.44	95.87	1078.82	0.00
8					
9					
10	32.20	71.89	140.74	1023.67	0.00
11					
12				979.80	0.00
13					
14	134.81	14.30	129.30	2044.64	121.00
15					
16		0.00	57.16	2093.94	202.89
17					
18	202.85	0.00	47.04	2233.91	246.66
19					
20	165.97	0.00	47.04	3820.58	773.38

REFERENCES

- Aurilio, A., Mason, R. and Hemond, H.F. 1994. Speciation and fate of arsenic in three lakes of the aberjona watershed. *Environ Sci Technol.* 28: 577-585.
- Broenkow, W.W. 1969. An interface sampler using spring-actuated syringes. *Limnology and Oceanography.* 14: 288-291.
- Donoghue, T., Ledwell, J.R., Doherty, K. 1998. *Water samplers for open ocean tracer release experiments.* Woods Hole, MA, Woods Hole Oceanographic Institution.
- Fallon, R.D., Harris, S., Hanson, S., and Brock, T.D. 1980. The role of methane in internal carbon cycling in Lake Mendota during summer stratification. *Limnology and Oceanography.* 25(2): 357-360.
- Harris, D.C. 1998. *Quantitative Chemical Analysis.* New York, W.H. Freeman and Company.
- Hemond, H.F. and Fechner-Levy, E. 2000. *Chemical Fate and Transport in the Environment.* San Diego, CA, Academic Press.
- Houser J, Bade D, Cole J and Pace M. 2003. The dual influences of dissolved organic carbon on hypolimnetic metabolism: organic substrate and photosynthetic reduction. *Biogeochemistry.* 64: 247-269.
- Ingvorsen, K. and Brock, T.D. 1982. Electron flow via sulfate reduction and methanogenesis in the anaerobic hypolimnion of Lake Mendota. *Limnology and Oceanography.* 27(3): 559-564.
- Kalff, J. 2002. *Limnology: inland water ecosystems.* Upper Saddle River, NJ, Prentice-Hall, Inc.
- Kampbell, D. and Vandegrift, S.A. 1998. Analysis of dissolved methane, ethane, and ethylene in ground water by a standard gas chromatographic technique. *Journal of Chromatographic Science.* 36: 253-256.
- Kelly, C.A., Rudd, J.W.M., Schindler, D.W. 1988. Carbon and electron flow via methanogenesis, SO_4^{2-} , NO_3^- , Fe^{3+} and Mn^{4+} reduction in the anoxic hypolimnia of three lakes. *Arch Hydrobiol Beih.* 31: 333-344.
- Liikanen, A., Flojt, L. and Martikainen, P. 2002. Gas dynamics in eutrophic lake sediments affected by oxygen, nitrate, and sulfate. *J. Environ. Qual.* 31: 338-349.
- Mattson, M. and Likens, G. 1993. Redox reactions of organic matter decomposition in a soft water lake. *Biogeochemistry.* 19: 149-172.

- Miller, J.C., Miller, J.N. 1984. *Statistics for Analytical Chemistry*. New York, John Wiley and Sons.
- Peters, Hayes, Hieftje. 1974. *Chemical Separations and Measurements*.
- Rudd, J.W.M. and Hamilton, R.D. 1978. Methane cycling in a eutrophic shield lake and its effects on whole lake metabolism. *Limnology and Oceanography*. 23(2): 337-348.
- Rudd, J.W.M. and Taylor, C.D. 1980. Methane Cycling in Aquatic Environments. *Advances in Aquatic Microbiology*. M. R. Droop, Jannasch, H.W. New York, Academic Press. 77-137.
- Rudd, J.W.M., Kelly, C.A., Furutani, A. 1986. The role of sulfate reduction in long term accumulation of organic and inorganic sulfur in lake sediments. *Limnology and Oceanography*. 31(6): 1281-1291.
- Schafran, G.C., Driscoll, C.T. 1987. Comparison of terrestrial and hypolimnetic sediment generation of acid neutralizing capacity for an acidic Adirondack lake. *Environ Sci Technol*. 21(10): 988-993.
- Senn, D. 2001. *Coupled arsenic, iron, and nitrogen cycling in arsenic-contaminated Upper Mystic Lake*. Cambridge, Massachusetts Institute of Technology. Ph.D.
- Senn, D. and Hemond, H. 2002. Nitrate controls on iron and arsenic in an urban lake. *Science*. 296: 2372-2375.
- Solorzano, L. 1969. Determination of ammonia in natural waters by the phenolhypochlorite method. *Limnology and Oceanography*. 14: 779-801.
- Splithoff, H.M., Hemond, H.F. 1996. History of toxic metal discharge to surface waters of the Adirondack Watershed. *Environ Sci Technol*. 30(1): 121-128.
- Splithoff, H.M., Mason, R., and Hemond, H.F. 1995. Interannual Variability in the Speciation and Mobility of Arsenic in a Dimictic Lake. *Environ. Sci. Technol*. 29: 2157-2161.
- Steenbergen, C.L.M. and Verdouw, H. 1984. Carbon mineralization in microaerobic and anaerobic strata of Lake Vechten (The Netherlands): diffusion flux calculations and sedimentation measurements. *Arch. Hydrobiol. Beih. Ergebn. Limnol*. 19: 183-190.
- Stookey, L. 1970. Ferrozine - A new spectrophotometric reagent for iron. *Analytical Chemistry*. 42(7): 779-781.
- Strayer, R.F. and Tiedje, J.M. 1978. In situ methane production in a small, hypereutrophic, hard-water lake: Loss of methane from sediments by vertical diffusion and ebullition. *Limnology and Oceanography*. 23(6): 1201-1206.

Swinnerton, J.W., Linnenbom, V.J. and Cheek, C.H. 1962. Determination of dissolved gases in aqueous solutions by gas chromatography. *Analytical Chemistry*. 34(4): 483-485.

Trowbridge, P.R. 1995. *Rapid redox transformations of arsenic and characterization of the internal seiches in the Upper Mystic Lake, Medford, Massachusetts*. Cambridge, Massachusetts Institute of Technology. M.S.

Wetzel, R.G. and Likens, G.E. 2000. *Limnological Analyses*. New York, Springer.